Construction and Building Materials 158 (2018) 961–984

Contents lists available at ScienceDirect

Construction and Building Materials

journal homepage: www.elsevier.com/locate/conbuildmat

Integrating geomatic approaches, Operational Modal Analysis, advanced numerical and updating methods to evaluate the current safety conditions of the historical Bôco Bridge

Álvaro Bautista-De Castro [a], Luis Javier Sánchez-Aparicio [a,*], Luís F. Ramos [b], José Sena-Cruz [b], Diego González-Aguilera [a]

[a] Department of Cartographic and Land Engineering, University of Salamanca, High Polytechnic School of Ávila, Hornos Caleros, 50, 05003 Ávila, Spain
[b] ISISE, Department of Civil Engineering, University of Minho, Campus de Azurém, 4800-058 Guimarães, Portugal

HIGHLIGHTS

- A multidisciplinary method was used to assess the safety conditions of the bridge.
- The bridge's model was placed in its longitudinal axis following a PCA analysis.
- The calibration strategy improved the results of the numerical simulations.
- The methodology can be applied to verify the load bearing capacity of bridges.

ARTICLE INFO

Article history:
Received 30 June 2017
Received in revised form 12 October 2017
Accepted 19 October 2017
Available online 5 November 2017

Keywords:
Historical bridge
Reinforcement concrete
Structural damage
Terrestrial laser scanner
Ambient vibration tests
Finite element model updating

ABSTRACT

This paper proposes a multidisciplinary approach, combining the terrestrial laser scanner, ambient vibration tests and minor destructive tests, to characterize an early reinforced concrete bridge in Portugal: the Bôco Bridge. All methods are complemented by advanced numerical simulations and a coarse to fine calibration strategy, based on the Douglas-Reid and the non-linear least squares approaches. Results obtained corroborate the robustness of the proposed approach, with an average relative error in frequencies of 1.2% and an average modal assurance criterion of 0.91. Considering this model, its current safety conditions were evaluated, obtaining a minimum safety factor of 2.1.

1. Introduction

Transportation networks are fundamental elements in the economic development of countries, facilitating the communication and trade between different places. Inside the wide diversity of infrastructures that compose these networks, bridges are necessary elements to overpass topographic accidents, such as rivers or gullies, being considered, as ones of the most common, expensive and vulnerable infrastructures [1].

Among the variety of materials utilized in the construction of bridges, from masonry to steel [2], reinforced concrete (RC) has been one of the most used construction material, especially after the development and popularization of the Hennebique [3] and Monier [4] systems in the beginning of the XXth century. This popularity has been mainly due to its high availability, good mechanical properties, (caused by the synergy between steel and concrete), moldability and relatively low maintenance costs among other factors [5]. However, the aggressive environments on which the concrete bridges are constructed (usually with presence of chlorides, melting salts and carbon dioxide), tend to degrade this structural material. This degradation is mainly governed by the destruction of the passivation layer (protection layer created between the concrete and steel bars promoted by the alkaline environment created into the concrete) due to the presence of chlorides from melting salts and carbonation from atmospheric CO_2 among other factors. Promoting the penetration of the water and the oxygen, the oxidation and volumetric expansion of the steel bars will

* Corresponding author.
E-mail addresses: alvarobautistadecastro@usal.es (Á. Bautista-De Castro), luisj@usal.es (L.J. Sánchez-Aparicio), lramos@civil.uminho.pt (L.F. Ramos), jsena@civil.uminho.pt (J. Sena-Cruz), daguilera@usal.es (D. González-Aguilera).

https://doi.org/10.1016/j.conbuildmat.2017.10.084
0950-0618/

be developed. Consequently, concrete cracking and concrete spalling and reduction on the mechanical adhesion between concrete and steel rebars will take place [6]. As a result, the bearing capacity of these infrastructures and their working life can be considerably reduced, being necessary to carry out accurate safety verifications in order to evaluate the response of existing structures to the current and new demands of traffic loads [7].

Added to this, the limited knowledge of the construction technology, the use of semi-empirical rules or the theoretical background of the engineering analysis, lead to a challenging topic in the study and preservation of historic RC bridges. Rigorous multidisciplinary approaches able to characterize the structures at different levels, mainly (i) at geometrical level; (ii) at structural level and; (iii) at material level, are required.

Regarding the geometry, geomatic sensors (e.g. terrestrial laser scanner or digital cameras) have been placed in a privileged position in the geometrical characterization of bridges, being possible the digitalization of these structures in a fast and accurate way [8,9]. However, the product of this digitalization, the point cloud, is limited to the extraction of sections and individual measurements through which the 3D model is created [9]. Not exploiting all the advantages offered by the new methods emerged into the reverse engineering field [10].

Concerning the structural and material characterizations, the use of the ambient vibration tests (AVT) as well as the use of in-situ and minor-destructive tests have been placed as the most feasible strategies to characterize bridges at these levels [7,9,11,12]. The results of these tests are later used into set-up advanced numerical simulations by means of the finite element method (FEM), allowing the evaluation of the structure under different casuistic (e.g. traffic loads or seismic actions) [12–14]. However, and behind the advantages offered by the FEM, the incorrect modelling of its geometry, boundary conditions, and mechanical properties may lead to erroneous results [14,15]. To avoid these unreliable results, different global optimization strategies can be applied, such as the particle swarm or the genetic algorithms [12], in order to minimize the discrepancies between the experimental and the numerical results, requiring in most of the cases, a large number of iterations in order to get reliable results and thus, large computational times [15]. In contrast with this limitation, different authors have been proposed the use local optimization strategies [9,14]. These methods use lower number of iterations to converge in a minimum, but needing a good initial approximation to ensure accurate results.

Considering the limitations previously detailed, the present paper proposes a multidisciplinary method, based on the combination of terrestrial laser scanning procedures, ambient vibration tests, laboratory tests, advanced numerical simulations, by means of FEM, and a robust cost-optimized calibration strategy based on the Douglas-Reid (approximation strategy) and non-linear least squares (local minimization approach) methods, with the aim of creating accurate numerical simulations. Simulations able to reproduce accurately the current safety conditions of these structures. Particularly, this methodology has been validated in the historical RC bridge constructed over the Cávado river: the Bôco Bridge located in Braga region, Portugal. This infrastructure was built in its origin according to the guidelines imposed by the Hennebique system in the year 1909 and later expanded, in order to withstand heavy traffic, in the year 1962. The low quality of the used concrete during this intervention has caused the degradation of its structural elements (mainly concrete spalling and steel corrosion), being necessary the evaluation of its current carrying capacity under the actual loading demand.

Within this context, the paper is organized as follows: after is initial Introduction, Section 2 briefly describes the study case, its historical background, constructive system and current state of conservation; Section 3 shows the experimental campaign carried out on the bridge; Section 4 presents the calibration of the numerical model; Section 5 details the safety analysis carried out; and finally, in Section 6 the conclusions are drawn.

2. The Bôco Bridge

2.1. Historical background

Located along the road EM595-1, connecting the regions of Amares and Vieira do Minho, the Bôco Bridge is the actual oldest RC bridge in use in Portugal. Erected between the years 1909 and 1910 by the company Moreira de Sá & Malevez, following the project designed by the architect Sebasião Lopes (Fig. 1a). In the year 1950, the bridge was analyzed by engineers of different institutions reporting its bad state of conservation. The main damages found were concrete spalling and corrosion of the reinforcements, specially on the arches and deck. Furthermore, the traffic was limited to a load of 5 tons per vehicle without crossing the bridge at the same time until the retrofitting took place. In September 1961, the rehabilitation works started, following the project designed by the engineer J. Duarte Carrilho. Project that was ended in 1962 and consisted on concrete jacketing by increasing the concrete sections and adding additional reinforcement to the different structural elements (Fig. 2) (Table 1) with amild steel S400-B [7], in contrast with the original steel that could be considered identical to the steel used in the Luiz Bandeira bridge (erected by the same company and following the same construction method) [11]: a Bessemer mild steel.

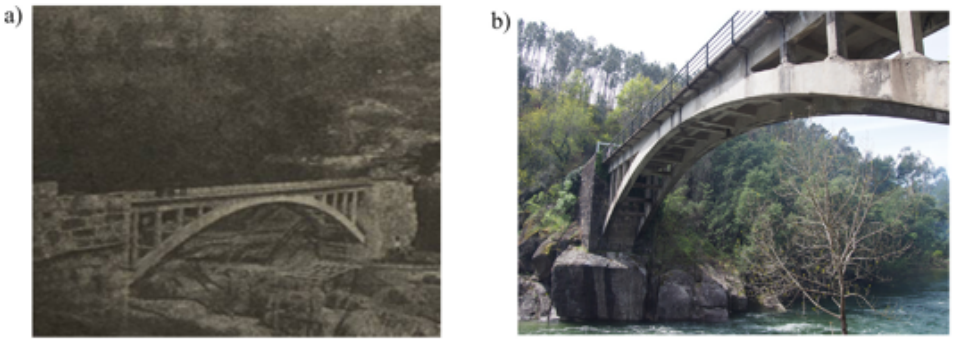

Fig. 1. General views of the RC bridge evaluated: a) Bôco bridge in the year 1910 [7] (original project); and b) current state of the Bôco Bridge.

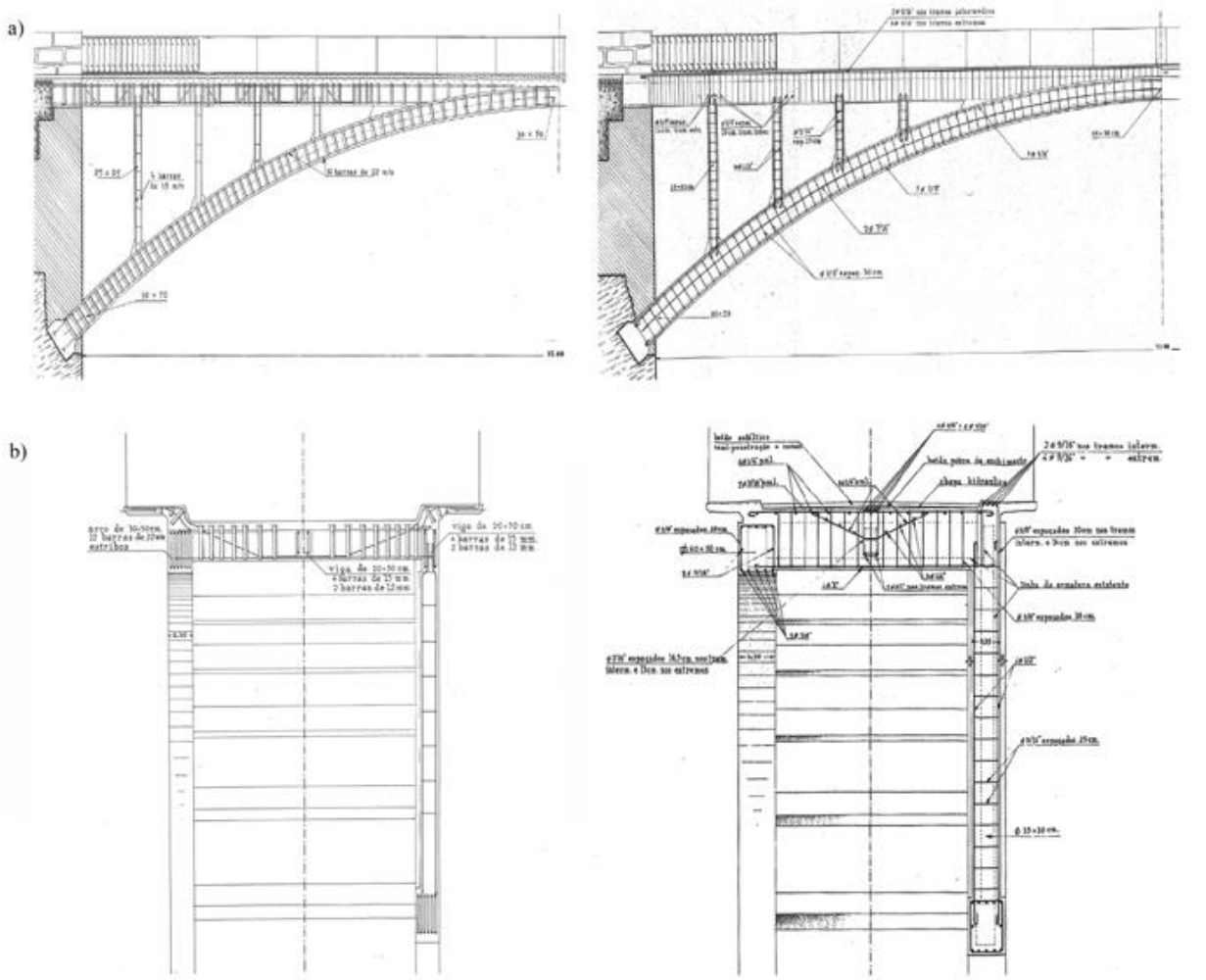

Fig. 2. Geometry and steel reinforcements of the Bôco Bridge [16]: a) downstream elevation before and after of the rehabilitation works; and b) cross-section of the deck before and after of the rehabilitation works.

2.2. Description of the bridge

The bridge is composed of seven different structural elements (Fig. 3): i) two arch girders with an average cross-section of 500 × 725 mm^2 (variable from their ends to the mid-span) and 35 m length, embedded its extreme in mansory walls; ii) 16 pillars spaced from each other 2 m with a cross-section of 350 × 320 mm^2, passing the loads from the lateral longitudinal girders to the arch girders; iii) 10 rectangular girders of 2.5 m length between the arch girders, making the bridge more rigid in the transversal direction; iv) 16 transverse girders with 2.7 m length that are connected to the lateral longitudinal girders and the central girder, with a cross-section of 300 × 550 mm^2, performing the same role that the rectangular girders connected to the arch girders; v) one central girder with 33 m length and a cross-section of 300 × 350 mm^2, with the ends supported on the masonry wall; vi) two lateral and longitudinal girders of 33 m length with a cross-section of 300 × 550 mm^2, embedded into the vertical masonry walls (Fig. 2a); and, vii) a deck, composed by a concrete shell with 120 mm of thickness. Furthermore, the non-structural elements used in the bridge (Fig. 3) (Fig. 4) are: i) an overlay of dry joints granite blocks of 150 × 150 mm^2 with 130 mm of thickness placed on the concrete deck; ii) two pedestrian sidewalks of 750 mm wide; and iii) metallic parapets of 900 mm high placed on the pedestrian sidewalks.

As stated in Section 2.1, the current structural elements of the Bôco Bridge have been the result of two stages, showing each one two concrete layers, namely (Fig. 5): i) old concrete, from the original desing; and ii) new concrete, added during the rehabilitations works.

2.3. Visual inspection

Results derived from the visual inspection carried out in 2016 corroborated the presence of different visual indicators of alteration, namely (Figs. 6 and 7): i) concrete spalling in the new concrete layer of the most of the structural components; ii) salt crusts in the arch girders and some pillars due to the aggressiveness of the environment; iii) presence of moisture, promoted by the infiltration of water from the pavement and the vertical masonry walls to the structural elements; iv) corrosion of the steel bars on the arch girders, pillars and rectangular girders connected

Table 1
Original and current dimensions, reinforcement bars and stirrups of the different structural elements of the Bôco Bridge [7].

Structural element	Original dimensions (mm)	Original reinforcement bars (mm)	Hennebique curved plates (mm)	Current dimensions (mm)	Added reinforcement bars (inches)	Added stirrups (inches)
Longitudinal arch girders (mid-span)	300 × 500	12 Ø 22	12	500 × 600	10 Ø 5/8 + 2 Ø 7/16	Ø 3/8
Longitudinal arch girders (at the abutments)	300 × 700	12 Ø 22	12	500 × 850	10 Ø 5/8 + 2 Ø 7/16	Ø 3/8
Pillars	250 × 250	4 Ø 15	12	350 × 320	4 Ø 1/2	Ø 5/16
Transverse girders	200 × 350	4 Ø 15	12	300 × 550	4 Ø 1	Ø 3/8
Central girder	200 × 300	4 Ø 15	12	300 × 350	2 Ø 3/4	Ø 7/16
Lateral longitudinal girders	200 × 500	4 Ø 15	12	300 × 550	–	–

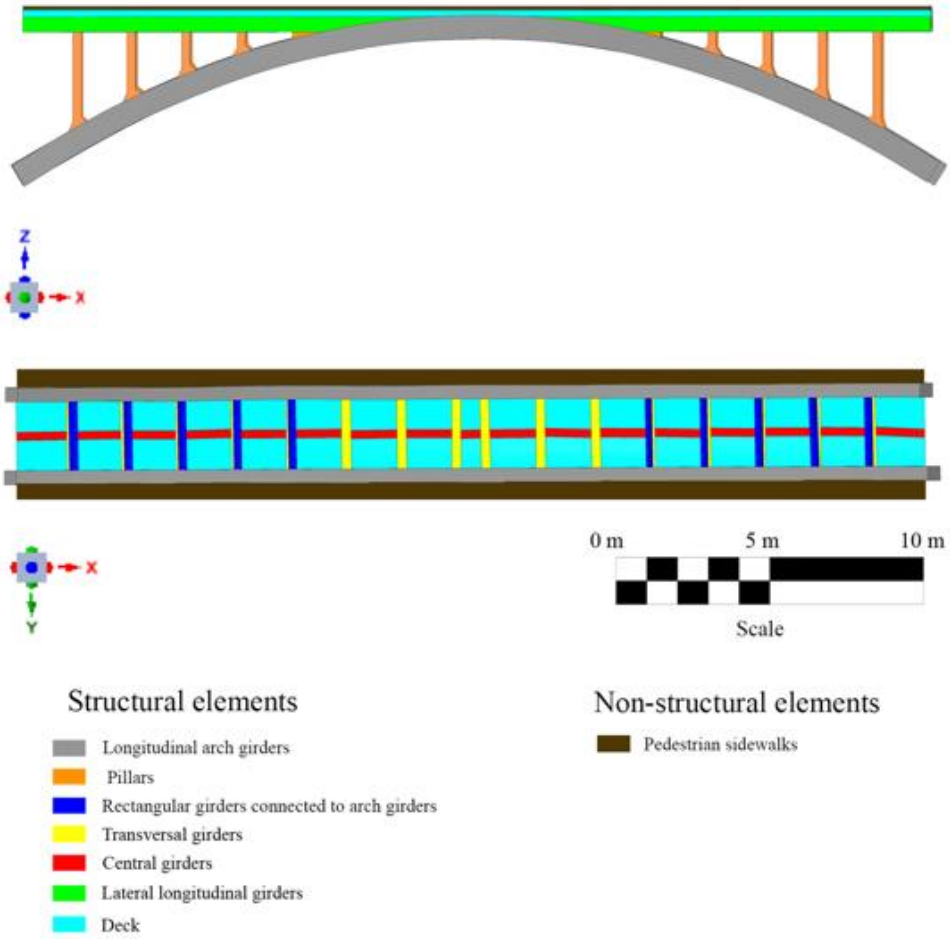

Fig. 3. Structural elements and non-structural elements of the Bôco Bridge.

to the arch girders; v) cracks on the connections between the arch girders and the vertical masonry walls; vi) algae in the arch girders and rectangular girders connected to the arch girders; vii) plants on the vertical masonry walls; viii) presence of lichen on a rectangular girder connected to the arch girders; and ix) moss on the arch girders, on a rectangular girder connected to the arch girders and on the vertical masonry walls. Part of these damages, more specifically the concrete spalling and steel bars corrosions, can be attributed to the high porosity (9.8% in contrast with the 3.2% of the old concrete layer) and the carbonation of the new concrete layer [7].

3. Experimental program: geometrical, dynamic and material characterization of the bridge

3.1. Geometrical characterization: Terrestrial laser scanner

Among the different digitalization strategies that can be used to reconstruct historical bridges [8,9], the terrestrial laser scanner (TLS) has been one of the more used, mostly due to it fast data acquisition, data processing, high accuracy and the absence of specific light conditions to acquire the data. Taking into account

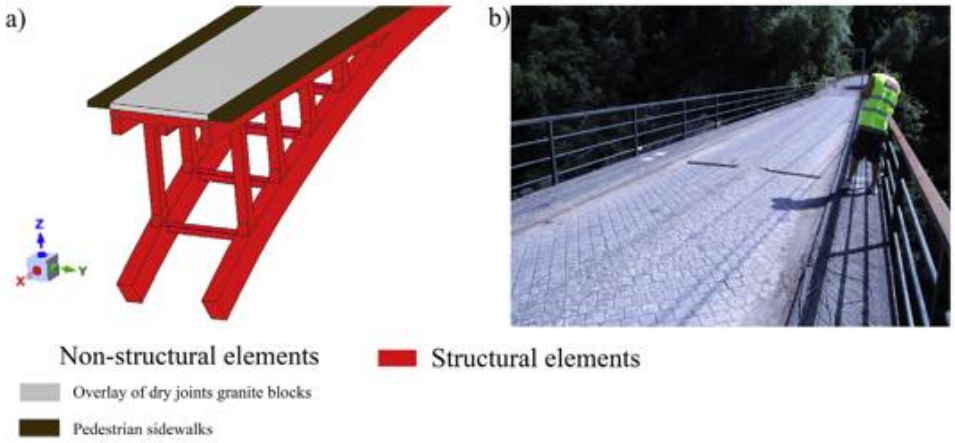

Fig. 4. Non-structural elements of the Bôco Bridge: a) Deck overlay composed by dry joints granite blocks and pedestrian sidewalks; and b) General view of the non-structural elements, overlay, pedestrian sidewalks and metallic parapets.

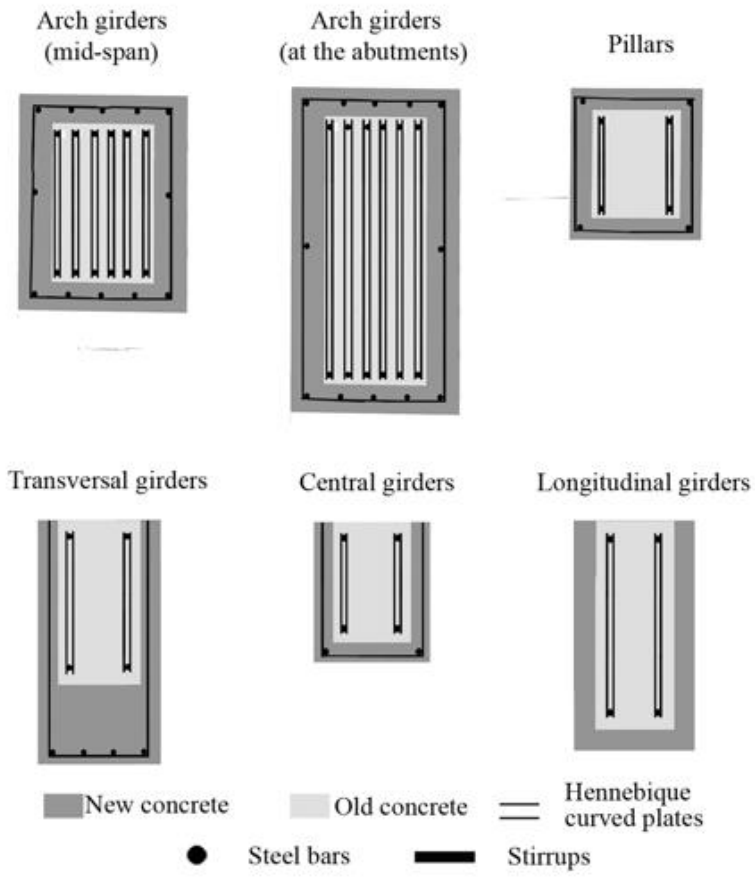

Fig. 5. Cross-sections with concrete layers and reinforcement (steel bars, stirrups and Hennenbique curved plates) of the structural components. Adapted from [7].

this, the lightweight Faro Focus 3D 120 TLS system (Table 2) (Fig. 8), based on the phase shift physical principle [17], was used to assess the geometry of the bridge.

Additionally to the TLS system, several registration spheres, with 20.0 cm and 14.5 cm of diameter (Fig. 8a), were used to align the different scans stations following the algorithm defined by [18].

As a result, 18 scan stations were needed to record the whole structure: i) 12 scans under the bridge; and ii) 6 scans on the bridge's deck, obtaining an alignment error of 0.003 ± 0.002 m. The huge amount of data captured, with a total of 672,316,191 points, required an optimization of the point cloud for further evaluations. In order to better manipulate the data, the following

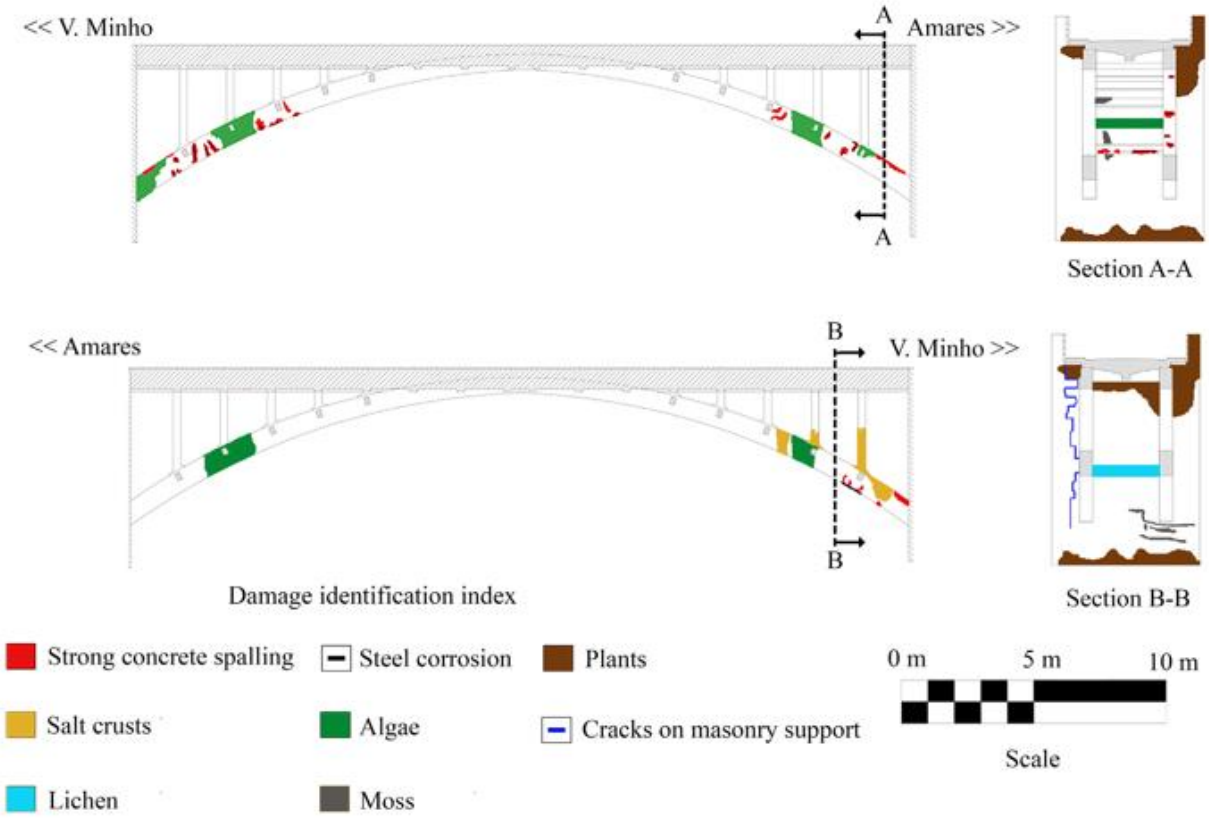

Fig. 6. Damage mapping obtained from the visual inspection carried out.

Fig. 7. Current state of conservation: a) extreme of an arch girder; b) concrete spalling on an arch girder; c) concrete spalling on a pillar; and d) cracks on the V. Minho vertical masonry wall.

Table 2
Technical specifications of the TLS Faro Focus 3D 120.

Faro Focus 3D 120	
Measurement principle	Phase shift
Measurement range	0.6–120 m
Accuracy nominal value	2 mm to 25 m in normal conditions of illumination and reflectivity
Field of view	360° Horizontal 305° Vertical
Capture rate	122,000/976,000 points
Beam divergence	0.19 mrad

decimation filters were applied: i) a distance filter with an average threshold of 40.0 m; and ii) a curvature-based decimation filter [19], with a threshold of 0.01 m, with the aim of simplifying flat areas while maintains relevant details, such as beam edges. As a result, an optimized 3D representation of the bridge was obtained made up by 9,853,819 points (1.47% of the original point cloud) (Fig. 9).

3.1.1. From the point cloud to the as-built CAD model

In the present dynamic identification and numerical evaluation of bridges the *x* and *y* axis were assumed as the longitudinal and transversal axis of the structure, respectively [7,15]. Being necessary the use of an additional procedure to place the bridge's point cloud in the correct coordinate system (Fig. 10). To this end, the following workflow was used: i) the evaluation of the covariance matrix of the point cloud; ii) the analysis of the Eigen-values and Eigen-vectors of the covariance matrix; and iii) the rotation of the point cloud considering the angle between *x* axis and third eigenvector (direction of maximum dispersion of the bridge).

With the aim of creating an accurate CAD model suitable for subsequent numerical evaluations, the multistep geometrical modelling strategy, proposed by [10] was considered which includes the following steps: i) Delaunay triangulation of the point cloud; ii) hole filling based on radial basis functions [20]; iii) topological noise removal by means of a local re-triangulation [21]; iv) segmentation of the different structural components and; v) adjustment of segmented elements into basic primitives based

Fig. 8. TLS and registration spheres used during the data acquisition: a) during the recording of the deck; and b) TLS surveying at the lower part of the bridge.

Fig. 9. 3D representation of the bridge resulting of the point cloud optimization.

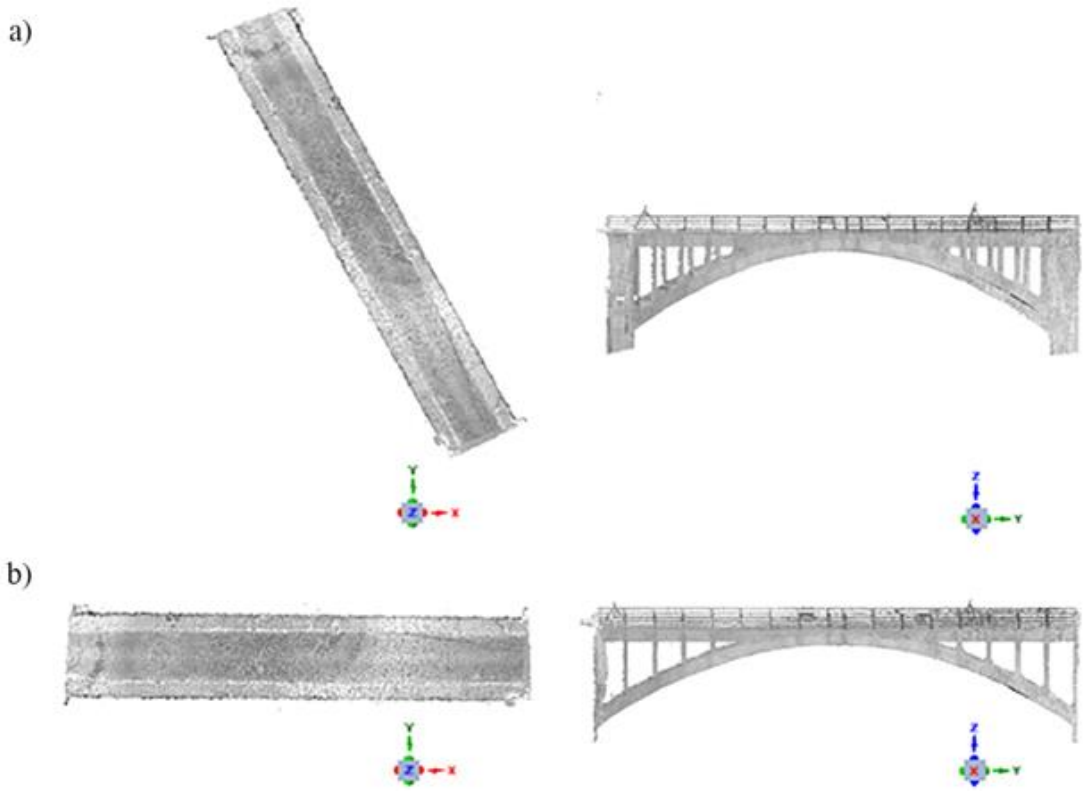

Fig. 10. Results derived from the methodology proposed: a) original point cloud; and b) rotated point cloud.

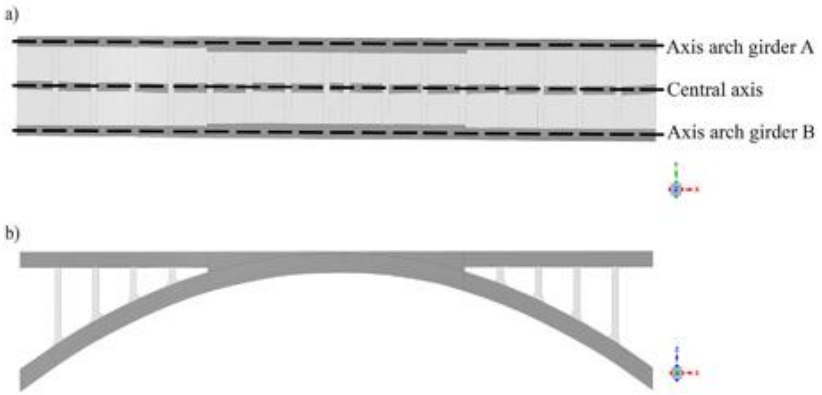

Fig. 11. As-built CAD model obtained by the proposed method: a) plant view (arches A and B); and b) elevation view.

on linear and non-linear (b-splines) extrusions. As a result, an as-built CAD model was obtained (Fig. 11), on which the geometrical deviations during the bridge construction were taken into account (Fig. 12).

3.2. Ambient vibration tests

A dynamical identification campaign, based on the Operational Modal Analysis (OMA) approach, was performed with the purpose of identifying the modal properties of the bridge (such as the frequencies, damping ratios and modal shapes). For a better results achievement, several numerical and previous dynamic analyses with different boundary conditions (Y-axis translation free and fixed) and mechanical properties were performed. These simulations allowed the proper configuration of the OMA tests (acquisition time and sampling rate) as well as the most suitable areas to place the accelerometers.

According to the obtained results, two setups with a total acquisition time of 20 min and a sampling rate of 256 Hz, were used. On each setup, a total of 14 uniaxial piezoelectric accelerometers, with a sensitivity of 10 V/g, range of ±0.5 g and 8 μg rms broadband resolution, were placed along the bridge's deck, being

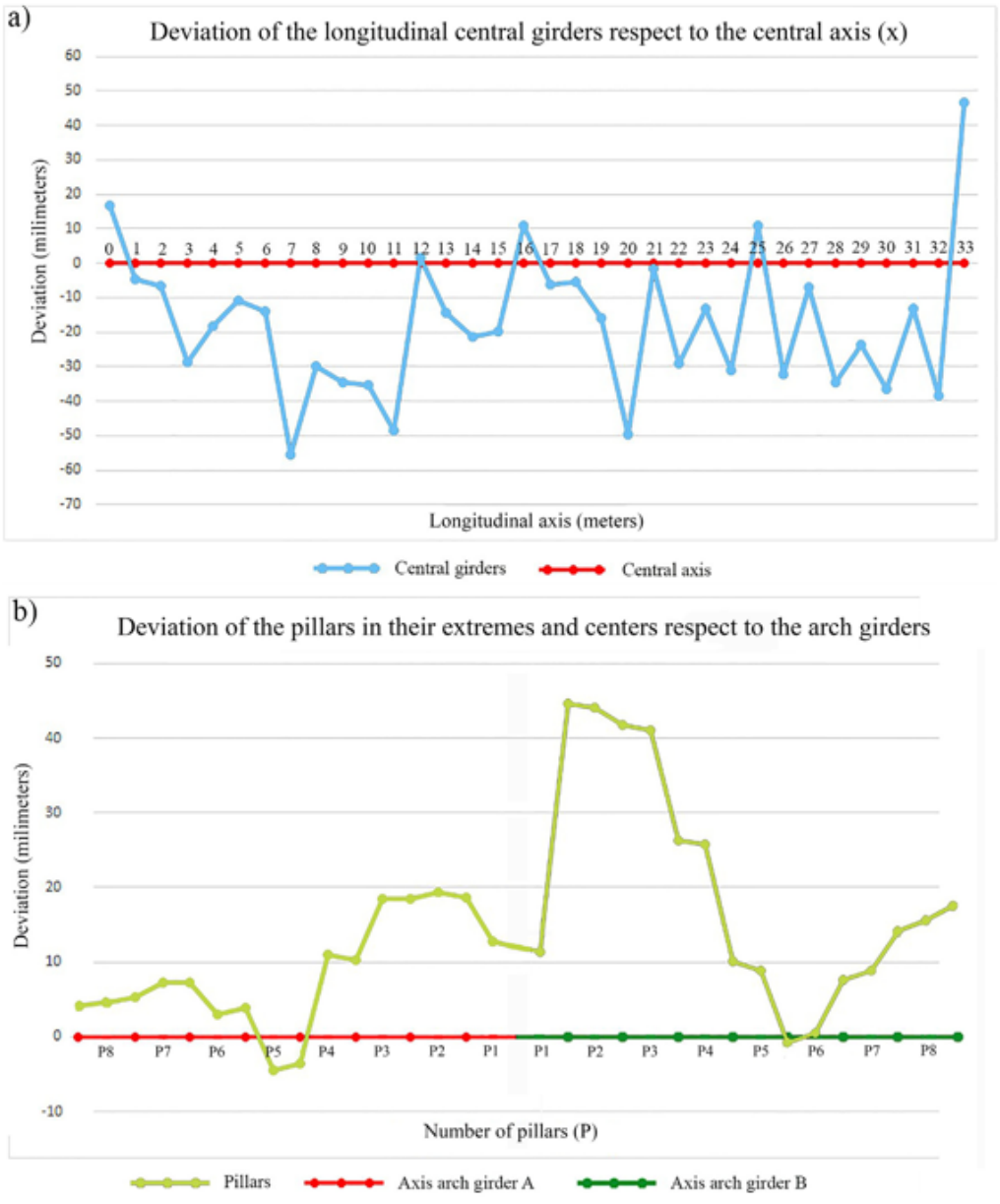

Fig. 12. Deviations of structural elements with respect to their theoretical positions: a) longitudinal central girders; and b) pillars.

5 of them considered as references (Fig. 13), namely accelerometers (3), (11), and (6) in the Z direction, and accelerometers (4) and (6) in the Y direction.

Finally, to extract the dynamic properties the Enhanced Frequency Domain Decomposition algorithm (EFDD), based on the power spectral density, was used to extract the mode shapes, natural frequencies and damping ratios [22]. As a result, 12 modes were identified with a range of frequencies between 4.15 Hz and 27.13 Hz (Table 3) (Fig. 14). The low coefficient of variation (CoV) for frequencies and damping ratios show the quality of the identified modal properties. On average, the damping ratio was equal to 1.67%.

3.3. Material characterization

Built in reinforced concrete, the Bôco Bridge shows in each structural component a total of two layers of concrete, namely: i) old concrete and ii) new concrete. According with this distribution, several mechanical and chemical tests were carried out in a previous experimental campaign to characterize the concrete and the steel of the bridge [7], by extracting samples from different locations as shown Fig. 15.

The average values for the elastic modulus of the new and old concrete (E_c) as well as their corresponding compressive strength ($f_{is,cyl}$) (Table 4) were obtained following the recommendations

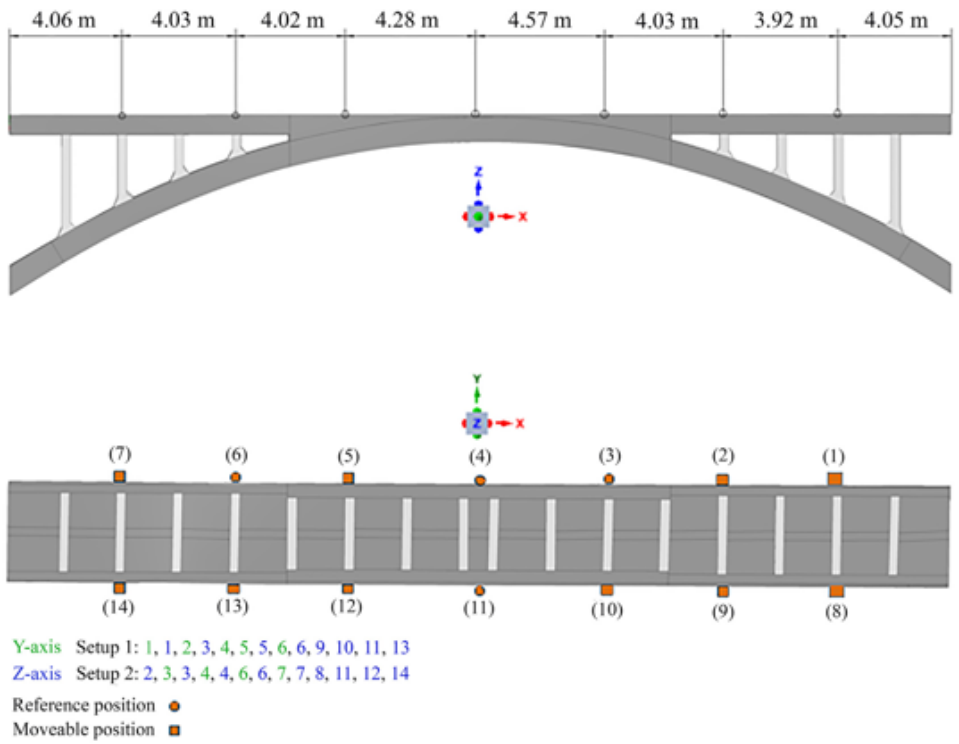

Fig. 13. Accelerometers positions and setups used during the ambient vibration tests.

Table 3
Natural frequencies and damping ratios obtained.

Mode shape	Frequencies (Hz)	CoV (%)	Damping ratios (%)	CoV (%)	Description
1	4.15	0.02	1.91	1.70	1st symmetrical translational (Y-axis)
2	6.51	<0.01	2.13	2.60	1st symmetrical vertical bending (Z-axis)
3	9.88	0.01	0.62	1.75	2nd asymmetrical vertical bending (Z-axis)
4	11.53	0.02	1.54	2.57	3rd asymmetrical vertical bending (Z-axis)
					2nd asymmetrical torsional (X-axis)
5	11.75	0.02	1.36	2.99	3rd asymmetrical torsional (X-axis)
6	12.34	0.01	2.47	2.41	2nd asymmetrical translational (Y-axis)
					4th asymmetrical torsional (X-axis)
7	14.11	0.04	2.43	6.15	5th asymmetrical torsional (X-axis)
8	18.71	0.03	3.95	3.13	4th asymmetrical vertical bending (Z-axis)
9	19.95	0.01	1.29	1.18	6th asymmetrical torsional (X-axis)
10	21.67	0.01	2.11	1.27	7th asymmetrical torsional (X-axis)
11	26.56	0.02	4.69	0.59	5th asymmetrical vertical bending (Z-axis)
12	27.13	0.01	1.70	0.98	8th asymmetrical torsional (X-axis)

exposed in LNEC E397:1993 [23] and NP EN 12390-3:2003 [24] respectively. From normalized cylinder of 150 mm of diameter and 300 mm of height, the following values were obtained: i) 41.30 GPa (with a coefficient of variation of 24.73%) and 52.1 MPa (with a coefficient of variation of 22.66%) for the old concrete; and ii) 27.25 GPa (with a coefficient of variation of 12.71%) and 21.1 MPa (with a coefficient of variation of 41.32%) for the new concrete.

In general the results derived from the physical, chemical and mechanical tests of the concrete used in the Bôco Bridge corroborated the low quality of the new concrete layer. In fact, this material shows a low compression resistance (Table 4) as well as a high porosity (around 9.8% with a coefficient of variation of 8.6%). This physical property, the porosity, has accelerated the carbonation effects and thus, steel corrosion and consequently concrete spalling along the different structural components of the bridge took place (Fig. 7) [7]. In contrast with this, the high elastic modulus and compressive strength and low level of porosity (3.2%) obtained for the old concrete layer suggests a high-quality concrete.

Regarding the steel used in the reinforcement bars, four samples were extracted and characterizing in laboratory using the following tests: i) scanning electron microscope with X-ray fluorescent spectrometer; and ii) carbon element tests. As a result, was possible to conclude that the steel used in the bridge was mild steel (presenting inclusions of manganese sulphide) [7].

4. Modelling the current state of the Bôco Bridge

Negative effects that bridges present, without a proper maintenance plan, can increase when time elapses, reducing its load capacity [26]. It is for this reason that is necessary not only to carry

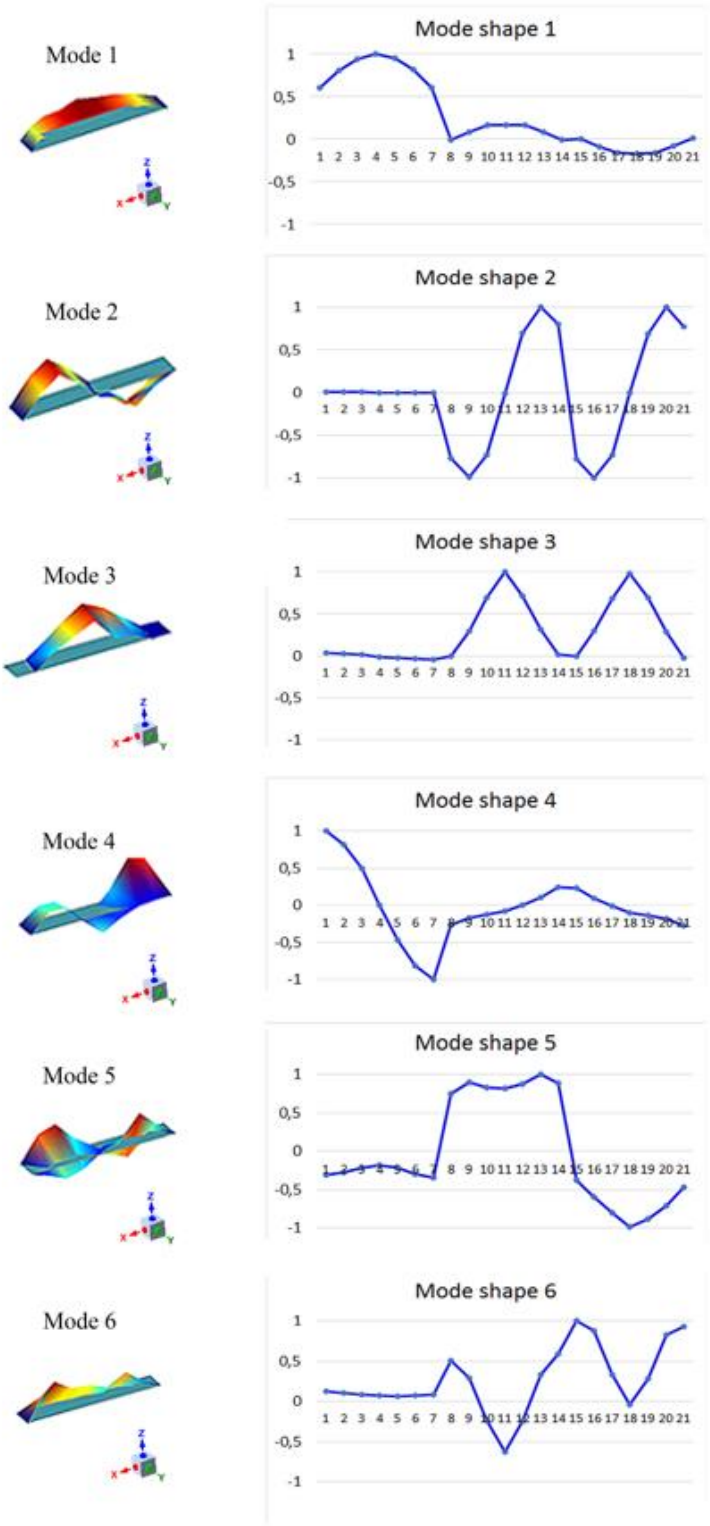

Fig. 14. Graphical representation of the first six vibrational modes extracted by the EFDD algorithm. In blue the experimental modal displacements. The horizontal axis of the graphs represent the degree of freedoms and the vertical axis the normalized modal displacements. (For interpretation of the references to colour in this figure legend, the reader is referred to the web version of this article.)

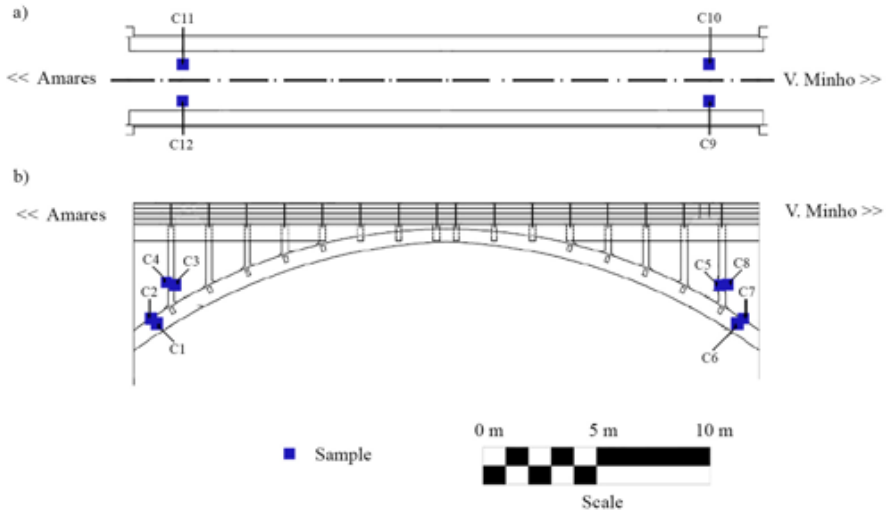

Fig. 15. Locations of the samples taken from the bridge by [7]: a) top view; and b) elevation view.

Table 4
Results obtained from the compression tests carried out by [7]. Young Modulus (E_c) of the new concrete have been estimated through the relation proposed by [25].

	Old concrete		New concrete	
Structural element	E_c (GPa)	$f_{is,cyl}$ (MPa)	E_c (GPa)	$f_{is,cyl}$ (MPa)
Arch (C1)	–	–	24.8	14.9
Deck (C10)	–	–	29.7	27.2
Pillar (C3)	54.1	58.8	–	–
Pillar (C4)	45.7	48.0	–	–
Pillar (C5)	–	59.2	–	–
Arch (C6.2)	43.2	58.0	–	–
Deck (C9)	36.6	29.9	–	–
Deck (C11)	–	64.8	–	–
Deck (C12.2)	26.7	46.1	–	–

out extensive experimental campaigns, focused on the characterization of the different structural components, damages or mechanical properties, but also numerical simulations to evaluate the current safety conditions of the bridge. These models need to be contrasted with experimental data, such as ambient vibration tests, to validate them.

4.1. Construction of the numerical model

According with the exposed above, a numerical simulation by means of FEM was carried out. To this end, the software TNO Diana ® [27] was used together with a numerical mesh composed of 193,814 elements (Fig. 16): i) 193,546 solid elements for the structural components and ii) 268 interface elements for the simulation of the interaction of the structure with its supports. The following constrains were considered: i) maximum size of the element 0.20 m; ii) minimum size of 0.05 m to represent properly the complexity of the as-built CAD model as well as to ensure a good quality of the different elements and; iii) at least 2 elements in the different structural components, with 4 elements in the z direction of the arch and longitudinal girders in order to capture possible non-linearities in further non-linear evaluations.

As it was described in Section 2, the different structural components of the bridge were retrofitted, showing each element two layers composed by concretes with different mechanical properties (Table 4). With the aim of reducing the complexity of the numerical simulation and thus, the computational effort, a homogenous concrete section was considered on each structural element. Therefore, the numerical model was divided in 5 groups of elements according with the similarity, in terms of concrete properties and structural components (Figs. 5 and 17).

To pass from the heterogeneous section (sections with two concrete layers) to the equivalent homogeneous section, the following variables were calculated: i) equivalent density; and ii) equivalent Young Modulus.

On one hand, the equivalent density of each group was calculated through the weighted arithmetic mean (considering as weight the percentage in volume of the two concrete in the structural element evaluated) (Fig. 3), taking into account as base values those obtained in the previous experimental campaign [7] (Table 5). On the other hand, the equivalent Young modulus of each group was obtained according following workflow depicted in Fig. 18.

The updated equivalent Young's modulus was computed as follows:

$$E_{updated} = E_{initial} \times \left(\frac{f_{i,j}^{ref}}{f_{i,j}^{num}} \right)^2 \quad (1)$$

where $E_{updated}$ is the calibrated equivalent Young Modulus; $E_{initial}$ is the initial value of the equivalent Young Modulus (homogenous section); $f_{i,j}^{ref}$ is the reference frequency (homogeneous section)

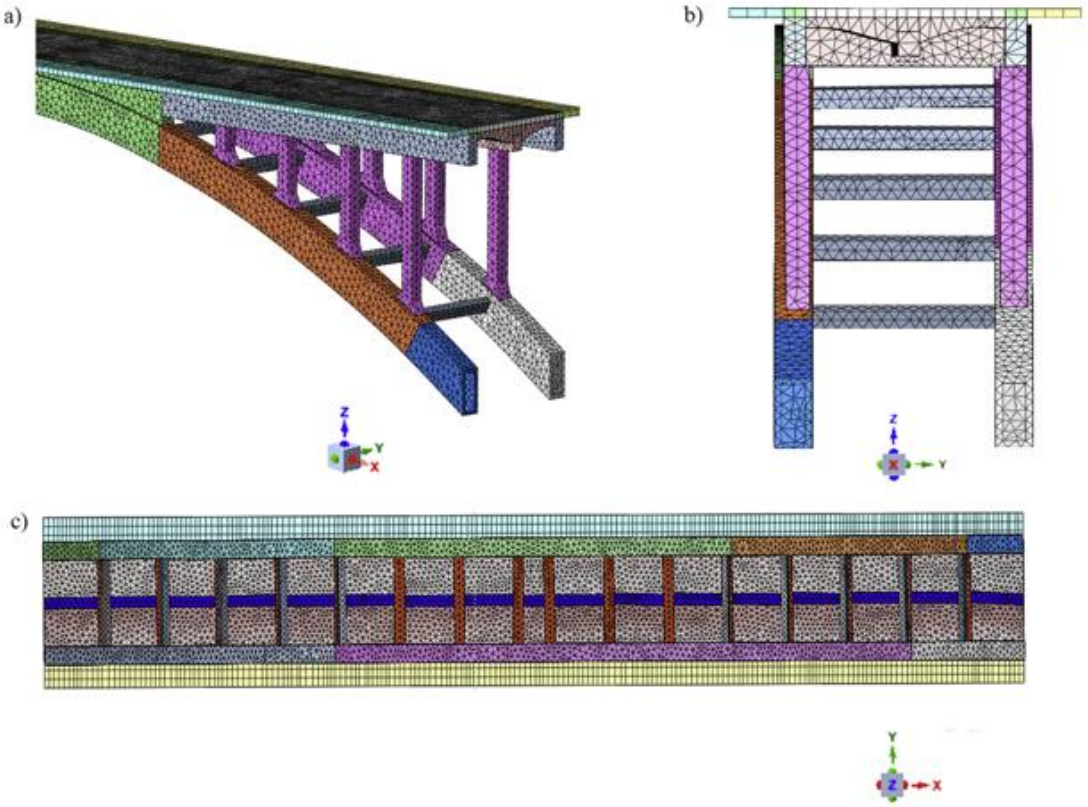

Fig. 16. Mesh of numerical model utilized: a) isometric view; b) front view and c) plant view.

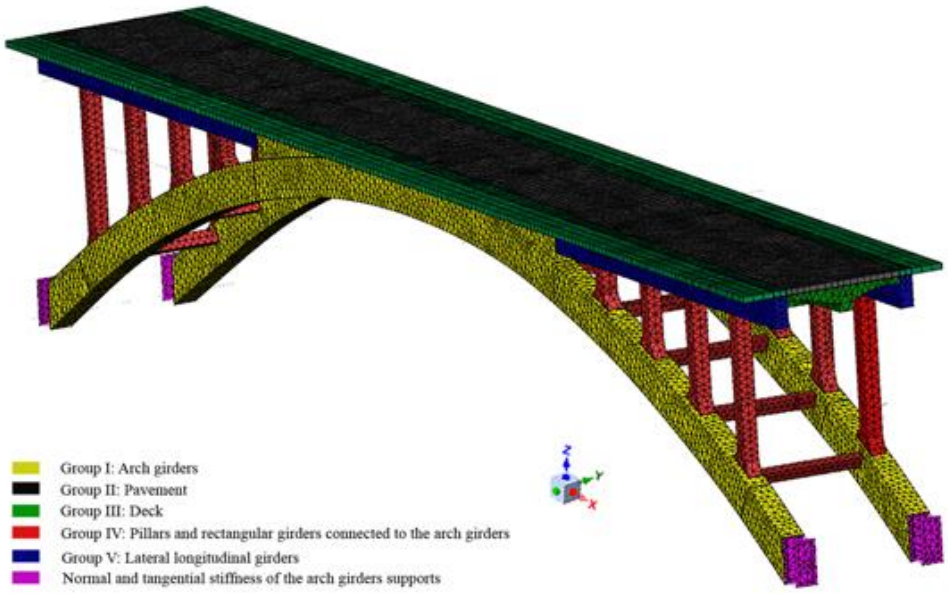

Fig. 17. Elements' groups considered during the calibration stage.

Table 5
Average, upper and lower Young Modulus and density values considered during the homogenization stage.

	Young modulus (GPa)		Density (kg/m^3)	
	Old concrete	New concrete	Old concrete	New concrete
Upper bound	62	34	2607	2217
Average	41	27	2418	2144
Lower bound	21	20	2229	2071

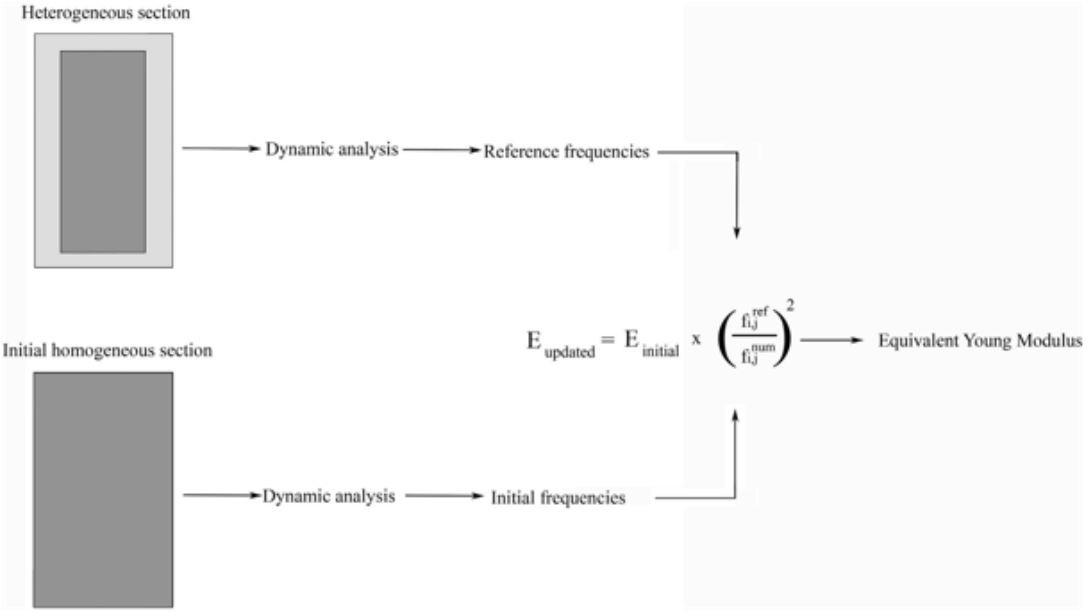

Fig. 18. Proposed workflow to obtain the equivalent Young modulus.

Table 6
Average, upper and lower equivalent Young Modulus and equivalent density values obtained during the homogenization stage.

		Upper bound	Average	Lower bound
Group I	*E* (GPa)	45	33	21
	Density (kg/m^3)	2412	2281	2150
Group III	*E* (GPa)	39	31	22
	Density (kg/m^3)	2500	2307	2114
Group IV	*E* (GPa)	30	22	13
	Density (kg/m^3)	2410	2297	2184
Group V	*E* (GPa)	33	24	15
	Density (kg/m^3)	2434	2310	2186

Table 7
Comparison between experimental and numerical frequencies and MAC values from the initial model.

Vibration modes	f_{exp} (Hz)	f_{num} (Hz)	Relative error (%)	MAC
1	4.15	5.52	32.96	0.85
2	6.52	6.31	3.07	0.97
3	9.88	10.77	8.97	0.97
4	11.53	13.61	18.06	0.75
5	11.81	26.07	120.76	0.85
6	12.34	13.69	10.92	0.81

obtained from the eigenvalue analysis of the group *i* (heterogeneous section) for the mode *j*; and $f_{i,j}^{num}$ is the frequency (homogeneous section) derived from the eigenvalue analysis of the group *i* for the mode *j*. As a result, the following equivalent values were obtained (Table 6) for the different groups considered. Concerning the Group II, the pavement ((granite blocks without mortar), the Young's modulus provided by [28] was considered equal to $E = 0.2 \pm 0.14$ GPa.

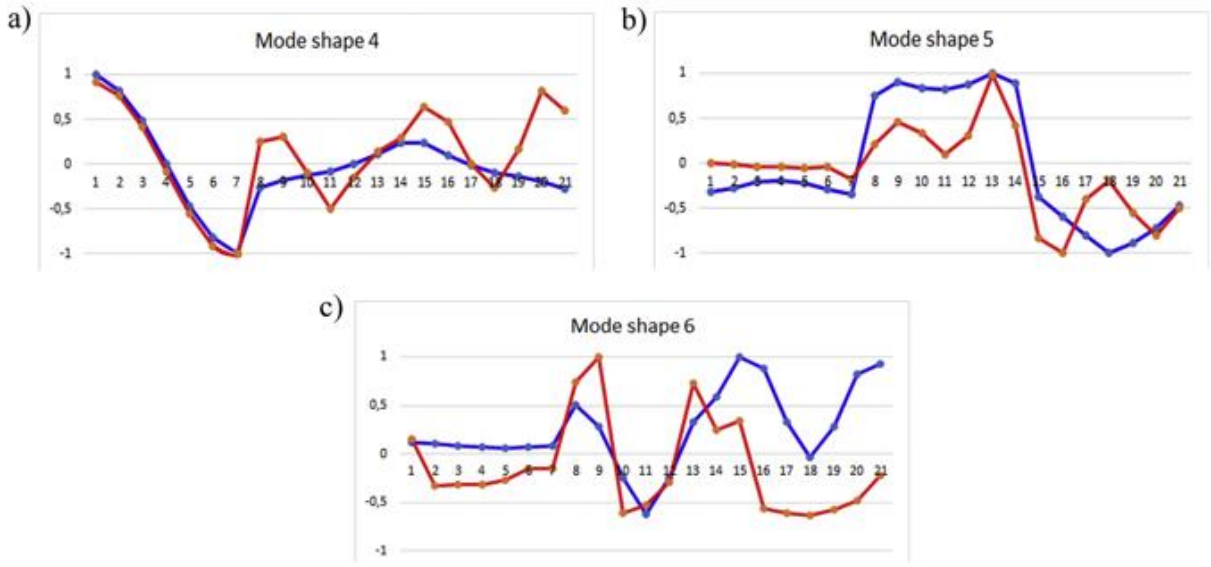

Fig. 19. Comparison between experimental and numerical modal displacements: a) mode shape 4; b) mode shape 5; and c) mode shape 6. In red the numerical modal displacements and in blue the experimental ones. The horizontal axis of the graphs represent the degree of freedoms and the vertical axis the normalized modal displacements. (For interpretation of the references to colour in this figure legend, the reader is referred to the web version of this article.)

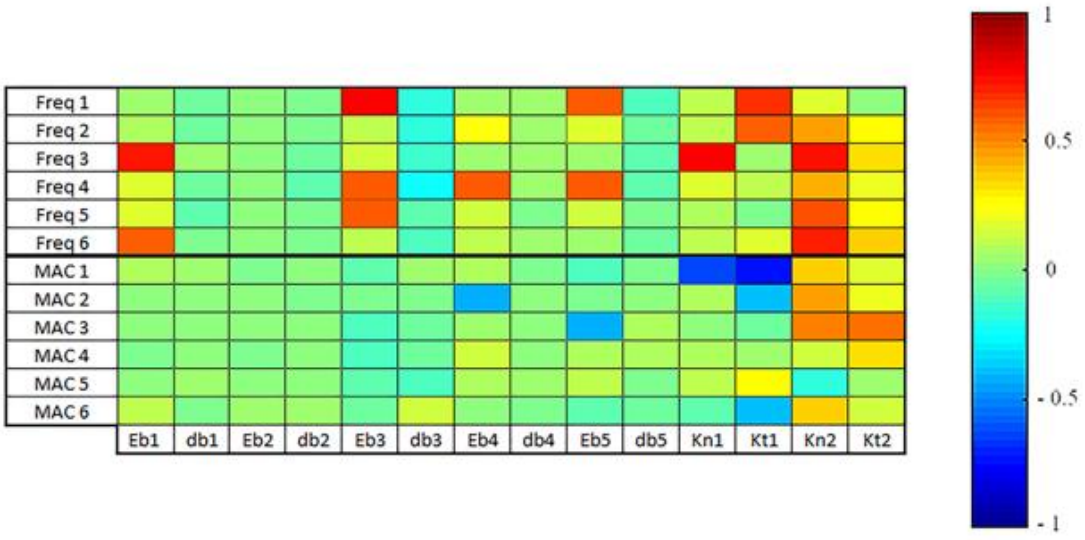

Fig. 20. Linear Spearman correlation matrix obtained during the first calibration (A).

Table 8
Updated values obtained during the DR and LS calibration.

Parameter	Upper bounds	Lower bounds	DR	LS
Eb1 (GPa)	47.95	20.59	31.08	29.96
Eb3 (GPa)	38.68	22.40	33.13	29.24
Eb4 (GPa)	29.63	22.79	29.52	28.66
Eb5 (GPa)	33.17	22.97	31.05	28.92
Kn1 (N/m^3)	1×10^{10}	1×10^{7}	1.91×10^{7}	1.36×10^{7}
Kt1 (N/m^3)	1×10^{10}	1×10^{7}	3.44×10^{8}	4.48×10^{8}
Kn2 (N/m^3)	1×10^{10}	1×10^{7}	6.14×10^{9}	6.35×10^{9}
Kt2 (N/m^3)	1×10^{10}	1×10^{7}	2.84×10^{9}	3.94×10^{9}

Table 9
Discrepancies obtained during the calibration A in terms of relative error in frequencies (f) and MAC values. In brackets, values achieved during the DR calibration.

Vibration modes	f_{exp} (Hz)	f_{num} (Hz)	Relative error (%)	MAC
1	4.15	4.19	1.02	0.93
		(4.21)	(1.42)	(0.94)
2	6.51	6.42	1.37	0.97
		(6.53)	(0.34)	(0.97)
3	9.88	9.53	3.55	0.97
		(10.04)	(1.63)	(0.97)
4	11.53	11.71	1.56	0.83
		(12.08)	(4.77)	(0.78)
5	11.81	11.57	2.05	0.88
		(12.90)	(9.23)	(0.88)
6	12.34	12.64	2.42	0.82
		(11.75)	(4.78)	(0.82)

4.2. Initial results

Taking into account the average equivalent Youngs' modulus obtained in Table 6, as well as the boundary conditions used during the evaluation of the Luiz Bandeira bridge erected in the same epoch and with the same construction system) [11], an initial evaluation was carried out.

To validate the accuracy of the numerical model, the relative error in frequencies and the modal assurance criterion (MAC) [29] were taken into account. Considering for these purpose, the first six frequencies and modal shapes (integrated by flexural and torsional modes). Results derived for this initial model shown a rigid structural system, especially in the transversal direction (modes 1,5,6) (Table 7), in comparison with the results obtained during the AVT.

Higher discrepancies were observer in the 4th and 6th vibrational mode (with MAC values of 0.75 and 0.81 respectively), arising from a bias, in terms of modal displacement, in the vicinity of the supports (Fig. 19). These discrepancies suggest a wrong modelling of the bridge's boundary conditions.

4.3. Finite element model updating strategy

As shown in the previous section, the first numerical simulation presented great discrepancies between the numerical and the experimental data, with an average relative error in frequencies of 32.46% and an average MAC value of 0.87, thus a calibration process able to minimize the discrepancies between the numerical and experimental modal responses was required.

From a mathematical point of view, the calibration of a numerical model can be considered as a constrained optimization problem [30], being possible to use two types of calibration methods: i) global optimization approaches or ii) local optimization algorithms. On one hand, the global optimization strategies can be used to find the global minimum of the cost function (function to be minimized), involving a high number of evaluations and thus large computational times, especially when the numerical model is complex [15]. On the other hand, local approaches can be used to find the nearest minimum of the cost function (which generally is a local minimum), using to this end a low number of evaluations, being more practical for complex simulations [14]. According with these premises, in this paper a coarse to fine calibration strategy is proposed of the following sequential stages: i) a global sensitivity analysis based on the Spearman correlation method [31] and the Latin hypercube sampling strategy [32] in order to evaluate the more sensible parameters; ii) a coarse calibration by means of the Douglas-Reid (DR) method [33] and the genetic algorithm [34]; and iii) a fine calibration through the non-linear least-squares strategy. Equation (2) define the cost function used during the calibration stage.

$$J = \frac{1}{2}\left[W_f \sum_{i=1}^{m}\left(\frac{f_i^{num} - f_i^{exp}}{f_i^{exp}}\right)^2 + W_{MAC}\sum_{i=1}^{m}(1 - MAC_i)^2\right] \quad (2)$$

where f_i^{num} and f_i^{exp} are the numerical and experimental frequencies for mode i respectively, MAC is the modal assurance criterion of the mode i, W_f is the frequency weight and W_{MAC} is the MAC weight. The values of one for the W_f and two for the W_{MAC} were considered

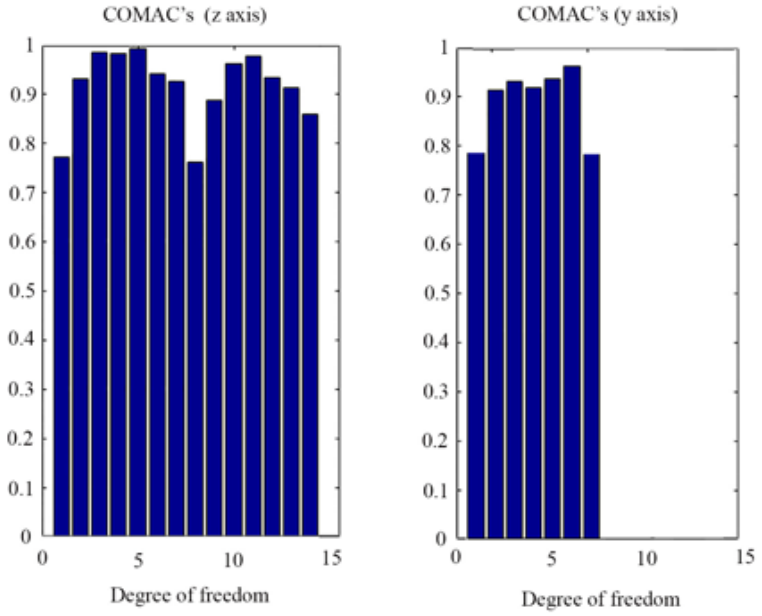

Fig. 21. COMAC values obtained during the first calibration: a) COMAC values in z axis; and b) COMAC values in y axis.

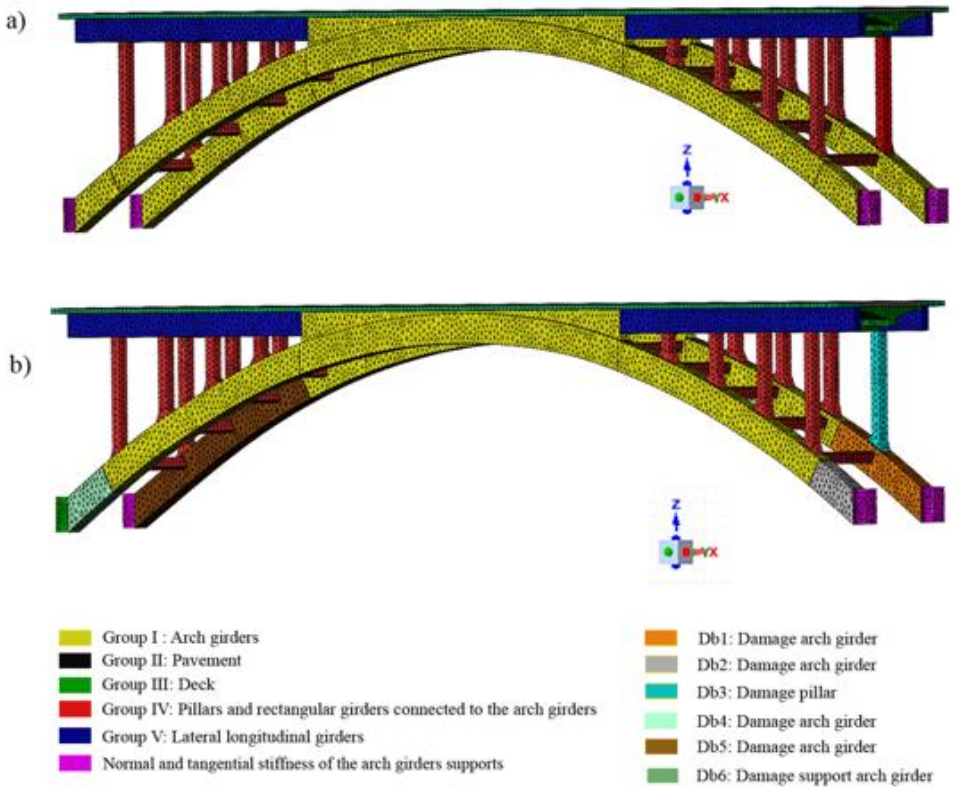

Fig. 22. Comparison between numerical models: a) numerical model 1; and b) numerical model 2.

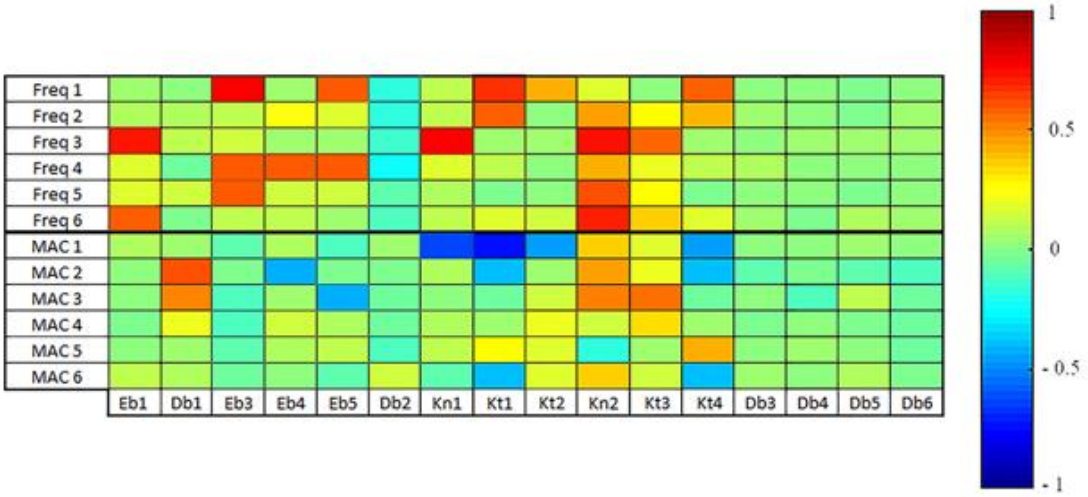

Fig. 23. Linear Spearman correlation matrix obtained during the second calibration (B).

in order to balance the contributions of the frequencies and MAC of the residuals of cost function.

With the cost function defined in (Eq. (2)), the DR algorithm was used to estimate the surface response (Eq. (3)), requiring a total of $2n + 1$ evaluations, being n the numerical variables to be calibrated.

$$R_i^{num} = \sum_{k=1}^{n}\left[A_{ik}X_k + B_{ik}X_k^2\right] + C_i \quad (3)$$

where R_i^{num} is the *ith* frequency or MAC values; A_{ik}, B_{ik} and C_i are the coefficients of the second order function; and X_k the k numerical variable applied during the calibration. Complementary to the DR algorithm, a genetic algorithm was applied to find the global minimum of the DR response surface. Finally, the global minimum of the DR response surface was refined through a the robust calibration method based on the non-linear least squares (LS), the

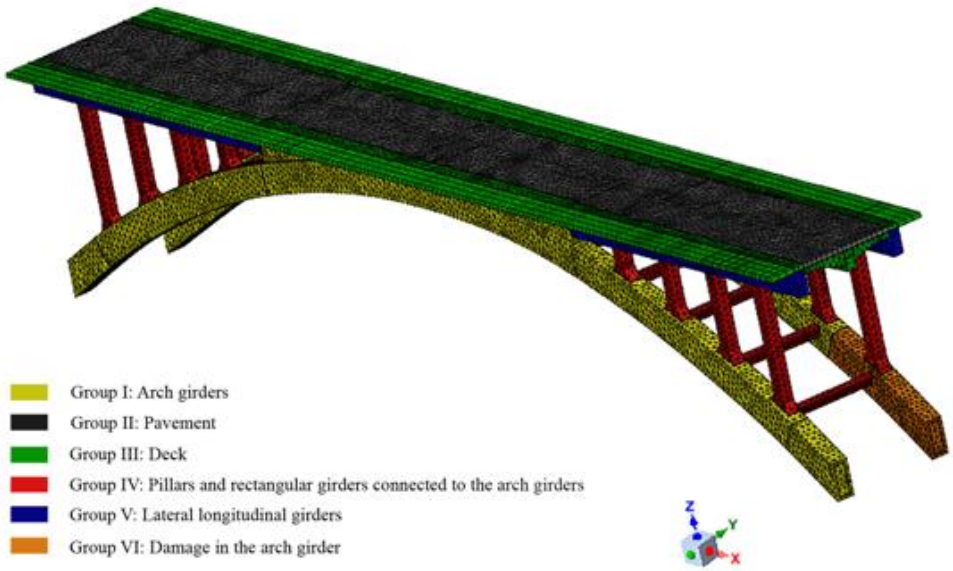

Fig. 24. Concrete groups considered during the second calibration (B).

Table 10
Discrepancies between the experimental and numerical data obtained during the second calibration stage (B). In brackets, the discrepancies of the initial model.

Vibration modes	f_{exp} (Hz)	f_{num} (Hz)	Relative error (%)	MAC
1	4.15	4.17 (5.52)	0.53 (32.96)	0.93 (0.85)
2	6.51	6.53 (6.31)	0.24 (3.07)	0.97 (0.97)
3	9.88	9.61 (10.77)	2.68 (8.97)	0.96 (0.97)
4	11.53	11.60 (13.61)	0.64 (18.06)	0.87 (0.75)
5	11.81	11.92 (26.07)	0.97 (120.76)	0.90 (0.85)
6	12.34	12.62 (13.69)	2.25 (10.92)	0.84 (0.81)

gradient-based Gauss Newton and the trust region reflective algorithms as exposed.

4.3.1. Numerical model 1: Calibration a

Considering the workflow proposed in the previous section, a global sensitivity analysis was carried out using 1500 samples (obtained through the Latin hypercube sampling method) and a total of 14 parameters, given by: i) five Young Modulus (*Eb1* to *Eb5*) and densities (*db1* to *db5*), representing the five groups previously defined (Fig. 14); ii) the normal and tangential stiffness of the deck supports (*Kn1* and *Kt1*); and iii) the normal and tangential stiffness of the arch girders supports (*Kn2* and *Kt2*).

On one hand, upper and lower bounds obtained in Table 6 were used as limits for the density and Young Modulus, respectively. On the other hand, and according with the literature [14,15,35,36], 1×10^{10} N/m^3 and 1×10^{7} N/m^3 were used as suitable upper and lower bounds, respectively, for the interface elements considered.

The sensitivity analysis (Fig. 20) revealed higher correlation coefficients, especially in the frequencies, between the dynamic response of the bridge and the support's stiffness (*Kn1, Kt1, Kn2 and Kt2*). These results corroborates the high relevance of the supports in the dynamic response of the structure in agreement with the conclusions obtained with the initial evaluation.

From the results obtained during the sensitivity analysis (Fig. 20), the following eight parameters were considered as suitable calibration variables: i) four Young Modulus, corresponding with the groups I, III, IV and V; and ii) the normal and tangential stiffness of the deck and arch girder supports.

As it was described in Section 4.3, the DR method and the genetic algorithm, with 50 individuals, 150 generations and a cross-over fraction of 0.8 according with the values used in similar works [12,37], was used to estimate the rough minimum of the cost function. The initial population used in the genetic algorithm was randomly generated by the Latin Hypercube sampling method. Finally, this minimum was refined with the LS method (Tables 8 and 9).

The average values of the calibration A (Table 8) for the relative error frequencies and MAC were 1.99% and 0.90, respectively. Comparing with the calibration performed by DR with the average values of the relative error frequencies and MAC, 3.70% and 0.89 were obtained, respectively. These results demonstrate that the LS method reduces the difference between numerical and experimental frequencies but doesn't significantly increases the MAC values.

To evaluate the possible origin of these discrepancies, the coordinate modal assurance criterion (COMAC) [29] was used. Results derived from this index show a concentration of discrepancies in the first, eighth, fifteenth and twenty-first degree of freedom (Fig. 21). These discrepancies correspond with the supports of the arch girders as well as the areas with higher concentration of damages (see Section 2.3 and Section 3.2).

4.3.2. Numerical model 2: Calibration B

Although the results obtained during the calibration A can be considered with acceptable accuracy (Table 9) (Fig. 17), a second calibration stage, named calibration B, was carried out with the aim to minimize discrepancies and to provide a more accurate numerical simulation.

Considering the results obtained during the AVT, with asymmetric modes (Fig. 14), as well as the high discrepancies observed in the first, eighth, fifteenth and twenty-first degrees of freedom (Fig. 17), additional parameters were introduced in the sensitivity analysis, namely (Fig. 22): i) damages in the arch girders, *db1, db2,*

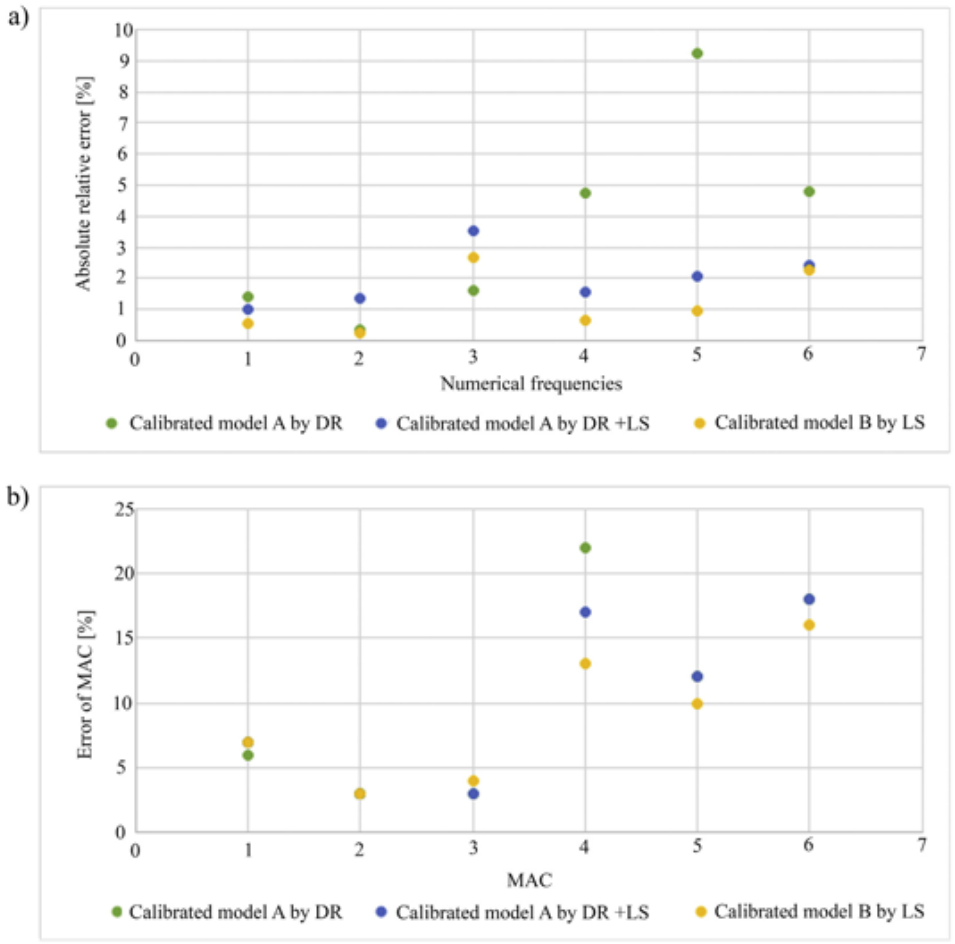

Fig. 25. Errors obtained during the different calibrations (A, B): a) Absolute relative error in frequencies; b) Relative error in MAC values.

Table 11
Updated values obtained during the different calibration stages.

Parameter	Upper bounds	Lower bounds	Calibration A	Calibration B
Eb1 (GPa)	47.95	20.59	29.96	29.79
Db1 (GPa)	47.95	20.59	29.96	27.80
Eb3 (GPa)	38.68	22.40	29.24	30.07
Eb4 (GPa)	29.63	22.79	28.66	27.92
Eb5 (GPa)	33.17	22.97	28.92	28.60
Kn1 (N/m^3)	1×10^{10}	1×10^{7}	1.36×10^{7}	1.04×10^{7}
Kt1 (N/m^3)	1×10^{10}	1×10^{7}	4.48×10^{8}	5.60×10^{8}
Kt2 (N/m^3)	1×10^{10}	1×10^{7}	4.48×10^{8}	4.22×10^{8}
Kn2 (N/m^3)	1×10^{10}	1×10^{7}	6.35×10^{9}	6.24×10^{9}
Kt3 (N/m^3)	1×10^{10}	1×10^{7}	3.94×10^{9}	4.34×10^{9}
Kt4 (N/m^3)	1×10^{10}	1×10^{7}	3.94×10^{9}	3.95×10^{9}

db4 and *db5* (Fig. 6) (Fig. 7a) (Fig. 7b); ii) damage in a support of the arch girder B, *db6* (Fig. 7d) and iii) damages in a pillar, *db3* (Fig. 7c).

From the evaluation of the Spearman correlation matrix (Fig. 23) two additional considerations were taken into account to improve the numerical calibration: i) the parameter *Db1*; and ii) an orthotropic behaviour of the supports. Therefore, in this analysis 12 calibration variables were considered (Fig. 24): i) 9 from the calibration A; ii) one variable that represent the damage on the arch girder; and iii) two additional shear stiffness on the deck and on arch girders supports. For this second calibration, only the robust calibration (LS method) was used. Using as starting values the results obtained during the calibration A. Thus, a more accurate simulation of the bridge, with an average relative error in frequencies of 1.2% and an average MAC value of 0.91 (Table 10) (Fig. 25), was obtained.

Concerning the updated parameters achieved in the different calibrations carried out (Table 11), especially the Young's Modulus variables (average value of 28.84 GPa), it is possible to corroborate a generalized damage of the new concrete layer observed during the visual inspection carried out (see Section 2.3) showed similar results that those obtained in Section 4.1 (average value of 30.81 GPa). In what regards to the calibrated stiffness, low values were obtained on the deck in the normal direction (1.04×10^7 N/m^3) with respect to the tangential stiffness (4.91×10^8 N/m^3) where obtained and higher values for the interfaces that define the interaction between the arch girders and the abutments (average value of 4.84×10^9 N/m^3).

Finally, Fig. 26 shows a graphical comparison between the experimental and numerical mode shapes. Analysing all results, one can conclude that the results derived from the second approach show a reasonable better correlation with the ones obtained from AVT (Figs. 25 and 26), especially for the

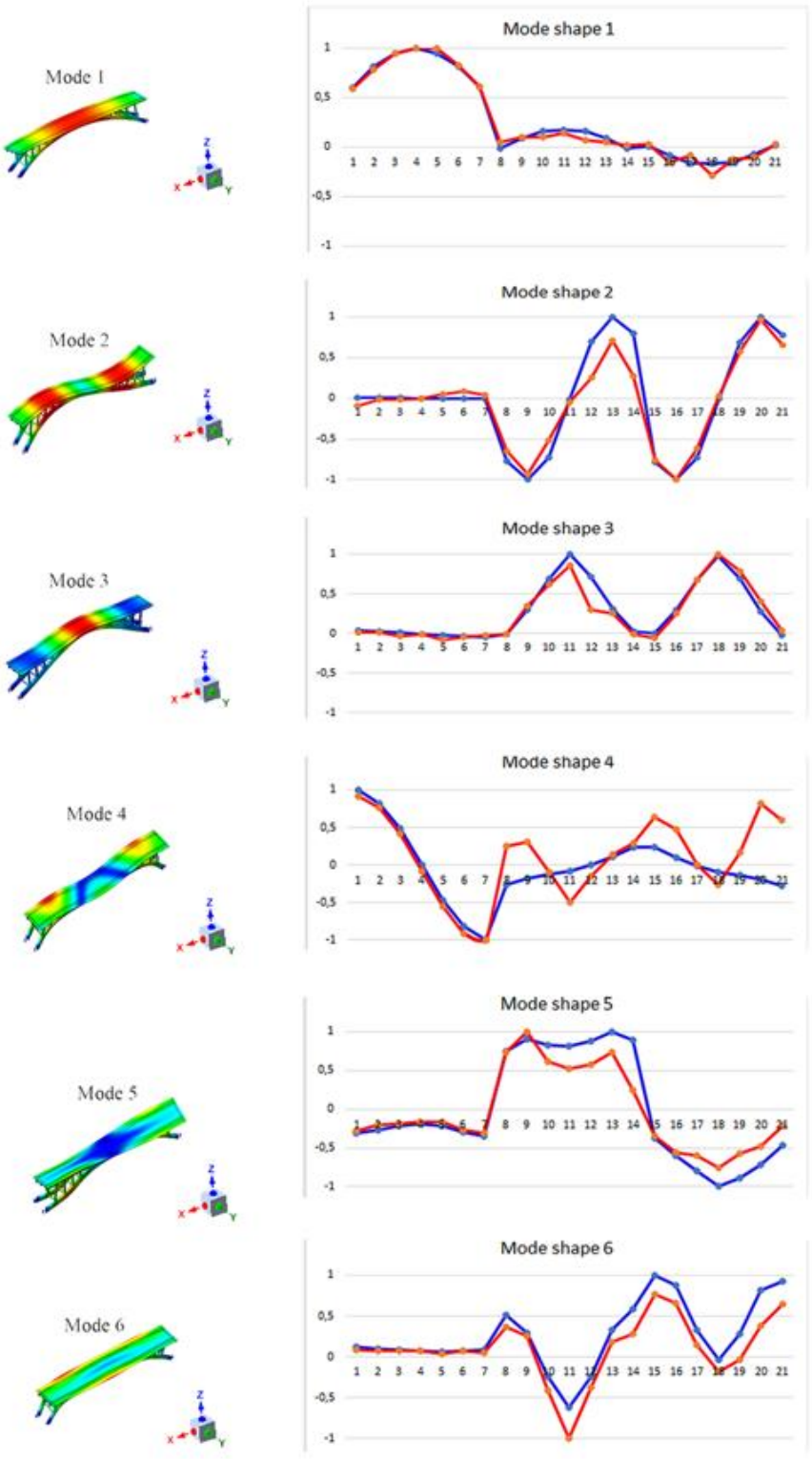

Fig. 26. Graphical comparison between experimental and numerical modal shapes obtained in the second.

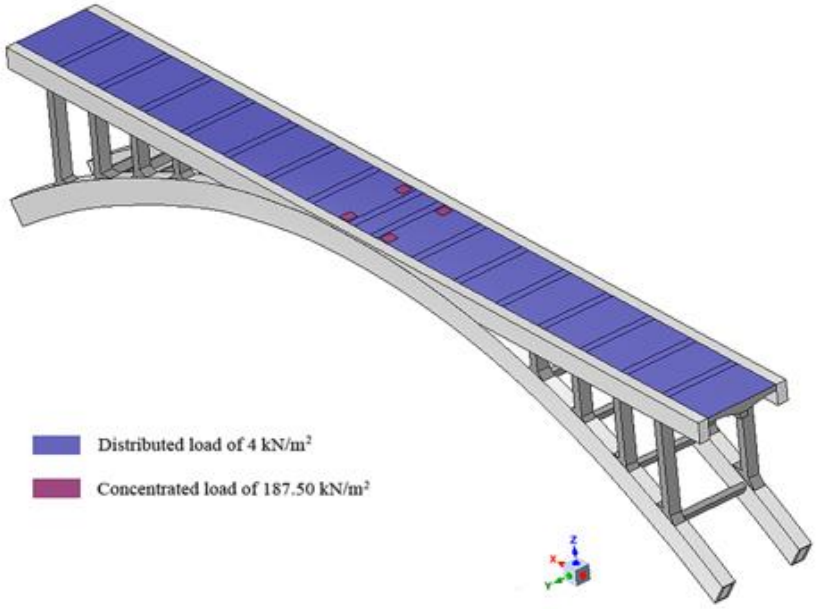

Fig. 27. Considered loads according with LM-1 of Eurocode.

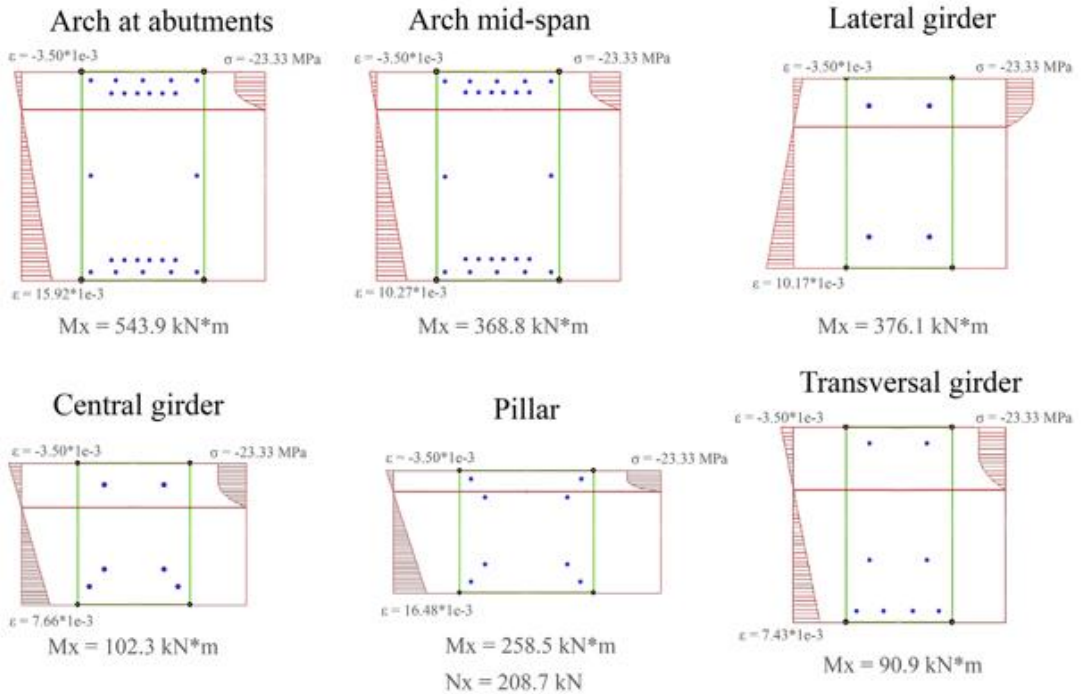

Fig. 28. Maximum flexural capacity of structural members and maximum compression axial force in the pillars. Results obtained by CSA analysis [42].

discrepancies observer in the 4th and 6th vibrational modes, corroborating the high influence of the boundary conditions in the dynamical response of the structure. It is worth mentioning that the discrepancies observed in the present numerical model that are concentred in local points (Fig. 26); can be attributed to the casting phases. These results requires further improvements of the numerical model.

5. Safety analysis

Considering the last calibrated model as the most accurate numerical representation of the bridge, an evaluation of the Ultimate Limit State (ULS) was carried out following the Eurocode recommendations [38–41]. During this evaluation, the maximum flexural capacity of each structural component and the

Table 12
Results obtained from the non-calibrated ideal model and the last calibrated numerical model during the static safety evaluation.

Structural elements	Action values of the ideal model	Action values of the calibrated model	Resistance values
$Mx_{Arch\_abutments}$	153.5 kN.m	180.3 kN.m	543.9 kN.m
$Mx_{Arch\_mid\text{-}span}$	125.3 kN.m	177.3 kN.m	368.8 kN.m
$Mx_{\_Lateral\ girder}$	64.4 kN.m	42.3 kN.m	376.1 kN.m
$Mx_{\_Central\ girder}$	18.9 kN.m	14.9 kN.m	102.3 kN.m
$Mx_{\_Pillar}$	57.6 kN.m	58.1 kN.m	258.5 kN.m
$N_{\_Pillar}$	67.6 kN	71.5 kN	208.7 kN
$Mx_{\_Transversal\ girder}$	30.3 kN.m	14.2 kN.m	90.9 kN.m

Table 13
Safety factors obtained from the ideal model and the last calibrated numerical model during the static safety evaluation.

Structural elements	Safety factors of the ideal model	Safety factors of the calibrated model
$Mx_{Arch\_abutments}$	3.5	3
$Mx_{Arch\_mid\text{-}span}$	2.9	2.1
$Mx_{\_Lateral\ girder}$	5.8	8.9
$Mx_{\_Central\ girder}$	5.4	6.9
$Mx_{\_Pillar}$	4.5	4.4
$N_{\_Pillar}$	3.1	2.9
$Mx_{\_Transversal\ girder}$	3	6.4

compression axial forces in the pillars were compared (resistance values) with the moments and the compression axial forces obtained by the numerical simulations (action values).

The static safety analysis was performed considering the current limitations of the bridge (maximum weight of 117.68 kN, maximum height of 3.50 m and 2.50 m of maximum width). A modification of the loads proposed in the Load Model 1 (LM-1) (Fig. 27) was considered [40], namely: i) gravity load; ii) LM-1 distributed load of 4.00 kN/m^2; and iii) LM-1 concentrated load of 187.50 kN/m^2 (area of the wheels of 0.16 m^2 according with LM-1 of Eurocode).

Loads were combined applying the Eurocode, where the safety factors for the most unfavourable case were considered (1.2 for gravity load and 1.5 for distributed load and concentrated load), obtaining the flexural moments of all structural elements and the compression axial force in the pillars (Fig. 28).

Results obtained from the safety evaluation shown that the most critical structural elements are the arch girders with a safety factor of 2.1 at the mid-span (Tables 12 and 13) (Fig. 29), verifying all the structural elements the ULS. These results were compared with those arose from a numerical simulation of an ideal model (model obtained from the historical plans and with the boundary conditions and material's properties considered in the first numerical simulation), showing large discrepancies, especially in the arch (17% more) and in the deck's girders (21% lower).

Regarding the seismic safety analysis, the desing ground acceleration was calculated according with the Eurocode 8 [43]. Being its value the results of the following considerations: i) a peak ground acceleration of 0.35 m/s^2; ii) a ground type A and; iii) an importance factor for buildings of 1. As a result, a desing ground acceleration of 0.35 m/s^2 was obtained, not being necessary the seismic verification of the bridge (0.35 m/s^2 < 0.04g, being g the gravity acceleration).

6. Conclusions

This paper proposed a multidisciplinary approach focused on the evaluation of the current safety conditions of historic bridges erected in reinforcement concrete. The method combines terrestrial laser scanning procedures, ambient vibration approaches, laboratory tests (e.g. scanning electron microscope and compression tests), advanced numerical simulation, by means of the FEM method, and a cost-optimized calibration strategy with the aim of characterizing the bridge at geometrical, material and structural level. With this approach several conclusions and advantages emerged when evaluating historic bridges, such as: i) the creation

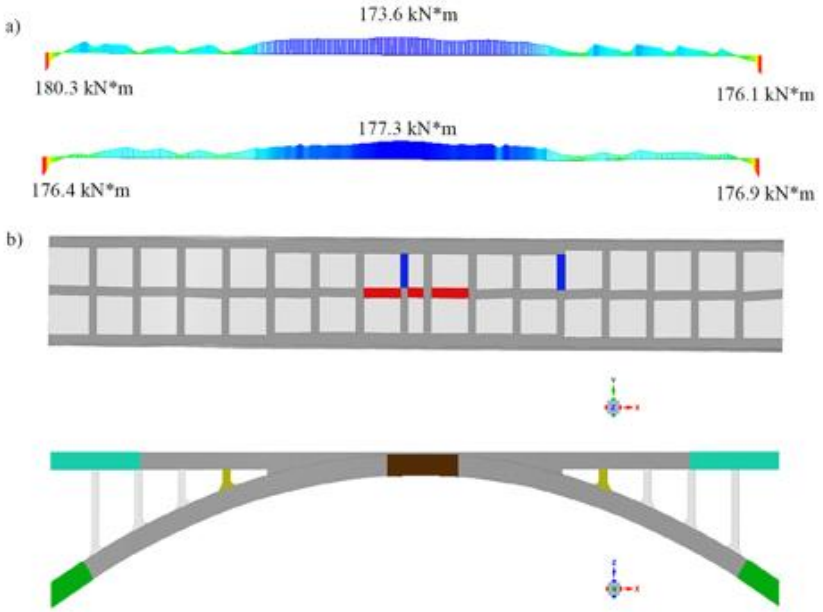

Fig. 29. Results obtained during the safety evaluation: a) graphical representation of the flexural moments (arch girders) obtained though the FEM; and b) structural components evaluated.

of as-built CAD models suitable for numerical simulations; ii) the automatic alignment between the geometrical data, the point cloud, and the data provided by the dynamic identification and; iii) the use of a cost-optimized calibration strategy.

To corroborate the robustness of the proposed method, an early reinforcement concrete bridge was chosen as study case: the Bôco Bridge in the north of Portugal. The method was able to create an accurate numerical simulation of the current state of the bridge, representing correctly the geometry of the structure, its material's properties and boundary conditions. The cost-optimized method used to calibrate the model, based on a coarse (DR and genetic algorithm) to fine (LS approach) methodology, allowed the reduction of the relative error in frequencies from an initial value of 32.46% to 1.22%, increasing the average MAC value from 0.87 to 0.91, spending a total of 5246 s (780 s in DR approximation and 4466 s during LS optimization) for the first calibration and 4704 s (only with LS method) for the second one in a processor Intel® XEON E3-1240 v3 at 3.4 Ghz and 8Gb RAM DDRII.

With respect to the safety conditions, the static analysis shown a bridge with enough capacity to bear the current solicitations on which the most critical structural part was the arch girder in mid-span with an estimated safety factor of 2.1 (value 17% lower than the safety factor obtained from a numerical simulation built with the ideal geometry, the average values of the concrete derived from the tests carried out and hypothetical support's conditions). Additionally, the studies carried out concluded that it is not necessary to take into account the seismic actions on the safety evaluation due to the low seismicity of the area.

Futures works will be focused on several fields: i) the application of additional NDT tests such as sonic and ultrasonic or rebar detector tests with the aim of improving the knowledge about the materials used in the Bôco Bridge; ii) the use of close-range aerial photogrammetry approaches (Unmanned Aerial Vehicles and Structure from Motion) to complement the TLS's point cloud with the aim of digitalizing all those areas not captured by this sensor (areas not visible from the ground); iii) the refinement of the numerical model according with the discrepancies observed in the second model calibration (punctual discrepancies), considering different the constructions and casting phases; iv) further calibrations including transient analysis with traffic actions and; v) nonlinear numerical evaluations by means of the push-over and the non-linear static analysis. Additionally, several radiometric classifications (by means of pixel-based approaches), based on the data captured by the TLS system, will be carried out to complete the damage diagnosis of the bridge.

Acknowledgments

This work was financed by ERDF funds through the V Sudoe Interreg program within the framework of the HeritageCARE project, Ref. SOE1/P5/P0258 and the Competitiveness Factors Operational Programme – COMPETE. This research has been also partially supported by CHT2 – Cultural Heritage through Time – funded by JPI CH Joint Call and supported by the Ministerio de Economia y Competitividad, Ref. PCIN-2015-071 and by national funds through FCT – Foundation for Science and Technology within the scope of the project POCI-01-0145-FEDER-007633.

References

[1] H. González-Jorge, D. Gonzalez-Aguilera, P. Rodriguez-Gonzalvez, P. Arias, Monitoring biological crusts in civil engineering structures using intensity data from terrestrial laser scanners, Constr. Build. Mater. 31 (2012) 119–128, https://doi.org/10.1016/j.conbuildmat.2011.12.053.
[2] F. Leonhardt, Bridges, 1984 ISBN: 0-262-12105-0.
[3] A. Hellebois, A. Launoy, C. Pierre, M. De Lanève, B. Espion, 100-year-old Hennebique concrete, from composition to performance, Constr. Build. Mater. 44 (2013) 149–160, https://doi.org/10.1016/j.conbuildmat.2013.03.017.
[4] J.-L. Bosc, J.-M. Chauveau, J. Clément, J. Degenne, B. Marrey, M. Paulin, Joseph Monier et la naissance du ciment armé, Ed. du Linteau 2001.
[5] M.L. Gambhir, Concrete Technology: Theory and Practice, Tata McGraw-Hill Education, 2013. ISBN: 1259062554, 9781259062551.
[6] F.P. Glasser, J. Marchand, E. Samson, Durability of concrete—degradation phenomena involving detrimental chemical reactions, Cem. Concr. Res. 38 (2) (2008) 226–246, https://doi.org/10.1016/j.cemconres.2007.09.015.
[7] J. Sena-Cruz, J.C. Araújo, F. Castro, M. Jorge, Assessment of the bôco historical RC bridge, SAHC2012–Structural Analysis of Historical Constructions (2012) 2214-2221 ISBN: 978-83-7125-216-7.
[8] M. Stavroulaki, B. Riveiro, G. Drosopoulos, M. Solla, P. Koutsianitis, G.E. Stavroulakis, Modelling and strength evaluation of masonry bridges using terrestrial photogrammetry and finite elements, Adv. Eng. Softw. 101 (2016) 136–148, https://doi.org/10.1016/j.advengsoft.2015.12.007.
[9] B. Conde, L.F. Ramos, D.V. Oliveira, B. Riveiro, M. Solla, Structural assessment of masonry arch bridges by combination of non-destructive testing techniques and three-dimensional numerical modelling: application to Vilanova bridge, Eng. Struct. 148 (2017) 621–638, https://doi.org/10.1016/j.engstruct.2017.07.011.
[10] M. Herrero-Huerta, D. González-Aguilera, P. Rodriguez-Gonzalvez, D. Hernández-López, Vineyard yield estimation by automatic 3D bunch modelling in field conditions, Comput. Electron. Agric. 110 (2015) 17–26, https://doi.org/10.1016/j.compag.2014.10.003.
[11] J. Sena-Cruz, R.M. Ferreira, L.F. Ramos, F. Fernandes, T. Miranda, F. Castro, Luiz Bandeira Bridge: assessment of a Historical Reinforced Concrete (RC) Bridge, Int. J. Archit. Heritage 7 (6) (2013) 628–652, https://doi.org/10.1080/15583058.2012.654895.
[12] D. Ribeiro, R. Calçada, R. Delgado, M. Brehm, V. Zabel, Finite element model updating of a bowstring-arch railway bridge based on experimental modal parameters, Eng. Struct. 40 (2012) 413–435, https://doi.org/10.1016/j.engstruct.2012.03.013.
[13] T. Türker, A. Bayraktar, Structural safety assessment of bowstring type RC arch bridges using ambient vibration testing and finite element model calibration, Measurement 58 (2014) 33–45, https://doi.org/10.1016/j.measurement.2014.08.002.
[14] L.J. Sánchez-Aparicio, L.F. Ramos, J. Sena-Cruz, J.O. Barros, B. Riveiro, Experimental and numerical approaches for structural assessment in new footbridge designs (SFRSCC–GFPR hybrid structure), Compos. Struct. 134 (2015) 95–105, https://doi.org/10.1016/j.compstruct.2015.07.041.
[15] T. Zordan, B. Briseghella, T. Liu, Finite element model updating of a tied-arch bridge using Douglas-Reid method and Rosenbrock optimization algorithm, J. Traffic Transp. Eng. (English Edition) 1 (4) (2014) 280–292, https://doi.org/10.1016/S2095-7564(15)30273-7.
[16] M.d.O. Publicas, "Ponte do Bôco" Direcção Geral dos Serviços de Urbanização, (1962).
[17] H. Yoon, H. Song, K. Park, A phase-shift laser scanner based on a time-counting method for high linearity performance, Rev. Sci. Instrum. 82 (7) (2011) 075108, https://doi.org/10.1063/1.3600456.
[18] A. Bienert, H.-G. Maas, Methods for the automatic geometric registration of terrestrial laser scanner point clouds in forest stands, Int. Arch. Photogramm. Remote Sens. Spatial Inf. Sci. 38 (part 3) (2009). W8.
[19] V.-S. Nguyen, A. Bac, M. Daniel, Simplification of 3D point clouds sampled from elevation surfaces, (2013) ISBN: 978-80-86943-75-6.
[20] D. Branch, L.C. Dang, N. Hall, W. Ketchum, M. Melakayil, J. Parrent, M. Troxel, D. Casebeer, D.J. Jeffery, E. Baron, Comparative direct analysis of type Ia supernova spectra. II. Maximum light, Publ. Astron. Soc. Pac. 118 (842) (2006) 560.
[21] I. Guskov, Z.J. Wood, Topological noise removal, 2001 Graphics Interface Proceedings: Ottawa, Canada, 19 (2001).
[22] R. Brincker, L. Zhang, P. Andersen, Modal identification from ambient responses using frequency domain decomposition, Proc. of the 18thInternational Modal Analysis Conference (IMAC), San Antonio, Texas, (2000).
[23] L.P. Standard, E397–1993, OPC concrete: Determination of elastic modulus in compression (1993).
[24] N. EN, 12390-3: 2003–Ensaios do betão endurecido, Resistência à compressão dos provetes. Lisboa.
[25] C.E. de Normalisation, EN 1992–1–1 Eurocode 2: Design of Concrete Structures, Part I-1: Generai Rules and Rules for Buildings, CEN, Brussels, 2004.
[26] N. Chouw, A. Pipinato, Dynamics of bridge structures, Innovative Bridge Des. Handb. (2016) 127–153.
[27] T. Diana, DIANA-finite element analysis, The Netherlands (2005).
[28] A. Kasahara, S. Matsuno, Estimation of apparent elastic modulus of concrete block layer, Proceedings of 3rd International Conference on Concrete Block Paving, 1988, pp. 142–147.
[29] R.J. Allemang, The modal assurance criterion–twenty years of use and abuse, Sound vib. 37 (8) (2003) 14–23.
[30] E. Simoen, G. De Roeck, G. Lombaert, Dealing with uncertainty in model updating for damage assessment: a review, Mech. Syst. Sig. Process. 56 (2015) 123–149, https://doi.org/10.1016/j.ymssp.2014.11.001.
[31] L. Myers, M.J. Sirois, Spearman Correlation Coefficients, Differences Between, Wiley StatsRef: Statistics Reference Online (2006), https://doi.org/10.1002/9781118445112.stat02802.

[32] M.D. McKay, R.J. Beckman, W.J. Conover, Comparison of three methods for selecting values of input variables in the analysis of output from a computer code, Technometrics 21 (2) (1979) 239–245, https://doi.org/10.1080/00401706.1979.10489755.
[33] B.M. Douglas, W.H. Reid, Dynamic tests and system identification of bridges, J. Struct. Div. 108 (ST10) (1982).
[34] D.E. Goldberg, Genetic algorithms, Pearson Education India 2006 ISBN: 817758829X, 9788177588293.
[35] X. Chen, P. Omenzetter, S. Beskhyroun, Calibration of the Finite Element Model of a Twelve-Span Prestressed Concrete Bridge Using Ambient Vibration Data, EWSHM-7th European Workshop on Structural Health Monitoring, 2014.
[36] D.-S. Jung, C.-Y. Kim, Finite element model updating on small-scale bridge model using the hybrid genetic algorithm, Struct. Infrastruct. Eng. 9 (5) (2013) 481–495, https://doi.org/10.1080/15732479.2011.564635.
[37] C. Costa, D. Ribeiro, P. Jorge, R. Silva, A. Arêde, R. Calçada, Calibration of the numerical model of a stone masonry railway bridge based on experimentally identified modal parameters, Eng. Struct. 123 (2016) 354–371, https://doi.org/10.1016/j.engstruct.2016.05.044.
[38] B.S. Institution, Eurocode 0 - Basis of structural design, BSI2004.
[39] E. STN Eurocode 1: Actions on structures, Part 1–1: General actions, Densities, self-weight, imposed loads for buildings, Slovak Office of Standards, Metrology and Testing (2007).
[40] C. Eurocode, 1: Actions on structures, Part 2: Traffic loads on bridges, Brussels: European Standard EN 2 (1991) 2003.
[41] C.R. Hendy, D.A. Smith, Designers' guide to EN 1992–2: Eurocode 2: design of concrete structures, Concr. Bridges (2007). Thomas Telford.
[42] H. Miranda, Á.F. Azevedo, J. Sena-Cruz, Cálculo orgânico de secções quaisquer em flexão desviada segundo o Eurocódigo 2, Encontro Nacional Betão Estrutural 2008: Actas (2008) 1–10.
[43] N. EN, 1 (2010) Eurocódigo 8: Projecto de estruturas para resistência aos sismos, Parte 1: Regras gerais, acções sísmicas e regras para edifícios, Lisboa: IPQ. 230p (1998).